PHILOSOPHICAL TRANSACTIONS OF THE ROYAL SOCIETY A MATHEMATICAL, PHYSICAL & ENGINEERING SCIENCES

The Impulse Breakdown Voltage and Time-Lag Characteristics of Long Gaps in Air. II. The Negative Discharge

R. T. Waters and R. E. Jones

Phil. Trans. R. Soc. Lond. A 1964 **256**, 213-234
doi: 10.1098/rsta.1964.0004

THE IMPULSE BREAKDOWN VOLTAGE AND TIME-LAG CHARACTERISTICS OF LONG GAPS IN AIR
II. THE NEGATIVE DISCHARGE

By R. T. WATERS* and R. E. JONES†

Research Laboratory, Associated Electrical Industries, Aldermaston Court, Aldermaston, Berkshire

(*Communicated by T. E. Allibone, F.R.S.—Received 22 February* 1963)

[Plates 10 to 15]

CONTENTS

Oscillographic measurement and time-resolved photographic recording have been used to examine the breakdown of rod/rod, rod/sphere and rod/plane gaps with long-duration negative impulse potentials of up to 1 MV crest.

As in the positive discharge, the breakdown process is found often to cease for considerable periods on the impulse wave tail. Breakdown then occurs after a long time lag for gaps composed of rod cathodes and rod or small sphere anodes. Where the anode is large, no long time lags are observed.

Measurement of the variation of breakdown strength with time during the impulse duration has been made by the superimposition of a second impulse upon the first, following a controllable delay. The results show a minimum probability of breakdown initiation after 15 μs of the applied impulse, and a subsequent slow recovery. It is suggested that this confirms the effect of the initial corona phase in causing space charge fouling of the gap.

* Now Senior Lecturer in the Department of Electrical Engineering, Welsh College of Advanced Technology, Cathays Park, Cardiff.

† Now at Elliott Bros (London) Ltd, Elstree Way, Borehamwood, Hertfordshire.

The breakdown voltage of rod/rod gaps is shown to decrease by up to 30 % when the impulse wave front is reduced from 0·50 to 0·06 μs. The breakdown strength with negative impulses is thus less than with positive impulses for wave fronts faster than 0·20 μs.

For the wave form 0·50/2000 μs, the breakdown voltage is found to depend more critically upon the dimensions of the earthed electrode than is the case with positive impulses. The breakdown voltage for a rod/25 cm sphere gap is 73 % greater than for a rod/rod gap, yet also 15 % greater than for a rod/plane gap. For gap lengths between 25 and 65 cm, the breakdown voltage of the rod/plane gap is found to increase with decreasing wave front duration.

The variation of the negative impulse corona with rate of potential rise and with crest voltage is examined photographically. Many of the observed variations of breakdown voltage and time-lag characteristics can be accounted for in terms of the impulse corona phase.

The time-resolved photography of the negative discharge over a wide range of conditions suggests that in the range of gap lengths investigated the formation of the positive leader rather than the negative leader is the necessary forerunner of sparkover.

1. Introduction

In part I of this paper it was emphasized that the mode of breakdown of air between electrode arrangements producing asymmetry in the axial electric field (one electrode being earthed) was dependent upon the polarity of the potential applied to the gap. The case where this potential is of impulse form and of negative polarity is of practical importance in high voltage transmission systems, where surges produced by the lightning hazard are largely of this kind. Again, since the lightning leader stroke itself is most often a discharge developing from a negatively charged cloud base, an examination of the negative polarity laboratory spark is of particular relevance.

In this second part, the results obtained from breakdown voltage and time-lag studies for negative impulses and various gap geometries are described; these are correlated with time-resolved photographs of the discharge, and contrasted with the behaviour observed with positive potentials.

2. Experimental methods

The methods used to produce and examine the discharge have already been described in part I. One additional method, however, has been used in this case.

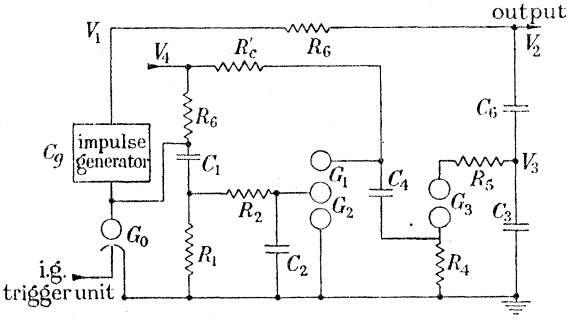

Figure 1. Superimposed-impulse generator.

A technique was devised to determine whether the breakdown strength of a rod/rod gap remained constant throughout the duration of an impulse potential. This consisted of applying to a rod/rod gap, already under stress, an additional impulse potential at a controllable time following the first voltage rise. Figure 1 shows the circuit arrangement.

Its operation was briefly this: G_0 was triggered to operate the impulse generator; the resultant charging of C_2 from C_1 then overvolted G_1. The time of collapse of G_1 could be controlled by its spacing and by the value of R_2. G_2 was arranged to break down following the collapse of G_1 .The ratio of the potential divider formed by C_6 and C_3 was such that $V_4 > 2V_3$. The operation of G_1 and G_2 then caused G_3 to break down, and charge sharing between C_3 and C_4 increased the output potential. R_6 was made large ($\sim 2000\ \Omega$) to reduce attenuation of the step voltage.

The circuit is analyzed in Appendix I.

3. Results

(*a*) *Corona discharge at a rod cathode*

An examination was made of the impulse corona discharge occurring at a hemispherically ended rod of 1·9 cm diameter opposed by an earthed plane with a separation of 300 cm.

The crest voltage of a 0·50/2000 μs impulse producing a discharge on 50% of applications was found to be 75 kV. This onset potential contrasted with the 90 kV which was found for positive impulses; the form of the discharge was also different from the positive case, consisting of a small glow of 0·8 cm extent at the electrode surface rather than a filamentary discharge. The brightness was also appreciably less than for positive corona at the same impulse level.

Upon increasing the crest voltage the discharge became of filamentary structure, and differences between the discharge produced by 0·20 and 0·50 μs wave-front potentials were found. The $f/1{\cdot}0$ camera was used to obtain the records of figure 2, plate 10. At 250 kV the impulse of wave front 0·20 μs produced a discharge some 25% more extensive (records (*a*) and (*b*)). At a crest voltage of 310 kV, however, a further change occurred (record (*c*)). The 0·50 μs wave front was found to cause the development of one to three channels of an extent of about 14 cm, while the remainder of the discharge was confined to a region within 4 cm of the electrode. The channels all showed a characteristic thickening some 6 cm from the electrode. The 0·20 μs wave front, on the other hand, showed no sudden change of structure at this level (figure 2(*d*)). As with the positive impulse corona, the discharge produced along the length of the rod was markedly more intense with the 0·20 μs wave front.

At 540 kV this basic difference between the 0·20 and 0·50 μs wave-front corona was again clear. The dual structure is again seen in figure 2(*e*). In the vicinity of the cathode there was a filamentary discharge envelope of roughly hemispherical form of radius 5·5 cm, centred on the cathode. The longer channels were then numerous and no longer showed the thickening of cross-section. They were branched towards the cathode at the cathode end as well as the anode-directed branching which took place along most of their length. These channels are conveniently called retrograde streamers. The 0·20 μs wave-front discharge again showed no such streamers.

At 700 kV, however, two of the five photographs obtained showed the retrograde streamers to be present even with a wave front of 0·20 μs (figure 2(*f*)). The channels appeared to terminate some 12 cm from the rod surface, but were connected to the electrode by a bundle of fine channels. The 0·50 μs wave-front case, as in figure 2(*g*), showed very numerous retrograde streamers, terminating near the cathode.

(b) *Rod/rod gaps*

(i) *Breakdown voltages and time lags*

In figure 3 are shown the impulse crest voltages required to produce 100% breakdown of the gap (curve 1) and the voltages just failing to cause breakdown on any application (curve 2). These were obtained with 0·50/2000 μs impulse wave shape. Curve 3 gives published results for 1·0/50 μs impulses, and curve 4 the breakdown voltages for 60 c/s potentials. The breakdown level of a 55 cm gap was found to be subject to day-to-day variations of $\pm 5\%$. Reproducibility at other gap lengths was of standard deviation $\pm 2\%$.

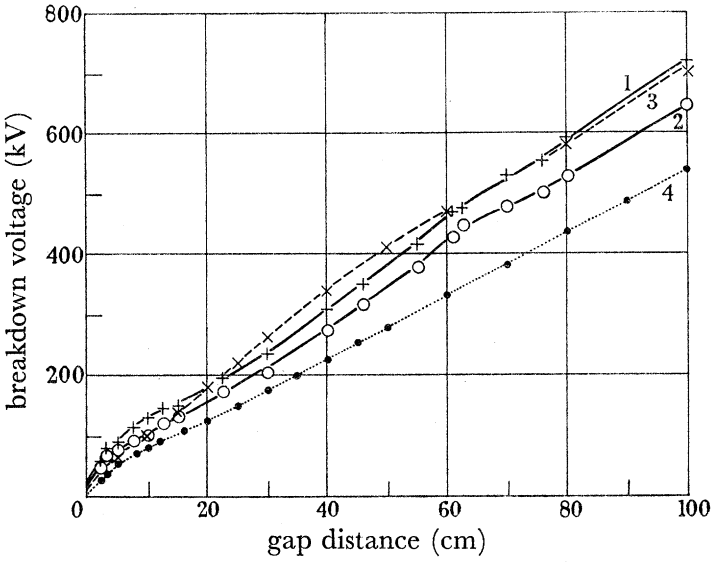

FIGURE 3. Breakdown voltages for rod/rod gaps. Curve 1, 100% breakdown, 0·50/2000 μs wave; 2, 0% breakdown, 0·50/2000 μs; 3, 50% breakdown, 1/50 μs (Allibone 1937); 4, 60 c/s a.c. breakdown (A.I.E.E. std. no. 4, 1940).

Time-lag measurements carried out in conjunction with the breakdown voltage experiments are displayed in figure 4. As was found with positive impulse the histograms show that, for gaps of 5 cm and above, two classes of breakdown were observed. Sparkover generally took place either with a short time lag of less than 20 μs or after a delay of 70 μs or more. Only at gaps in the range 10 to 30 cm did a few time lags fall between 20 and 70 μs, this period on the wave tail being designated as the dead-time.

The form of the time-lag distributions varied with crest voltage as in the positive discharge, i.e. a high proportion of long time-lag at potentials giving a low probability of breakdown, with higher voltages producing breakdowns of short time lag. With negative impulses, however, it was found that at voltages giving a high proportion of breakdowns of short time lag, occasional breakdowns of very long time lag arose once again. This behaviour was most marked at the longer ($\geqslant$ 70 cm) gaps.

It should again be emphasized that the long time lags observed were not due to any fluctuations of potential difference across the gap. It is well known that current-limiting resistance in series with a gap can increase the time to sparkover by interrupting discharge growth (Allibone & Meek 1938; Waters & Jones 1959). No series resistance in excess of the 800 Ω required to produce a damped output wave was used here and oscillographic recording of the gap voltage showed no fluctuations.

PHILOSOPHICAL TRANSACTIONS OF THE ROYAL SOCIETY A MATHEMATICAL, PHYSICAL & ENGINEERING SCIENCES

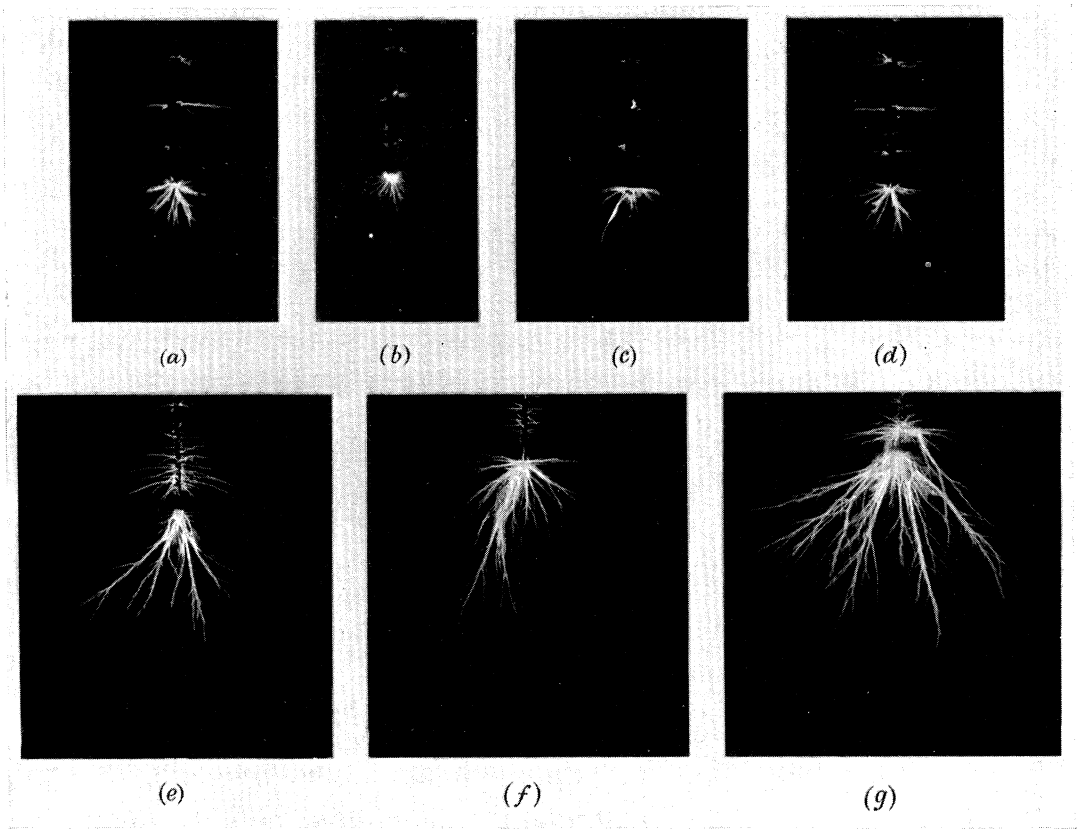

FIGURE 2. Impulse corona discharge at a rod-cathode: (*a*) 250 kV crest voltage, wave shape 0·20/2000 μs; (*b*) 250 kV crest voltage, wave shape 0·50/2000 μs; (*c*) 310 kV crest voltage, wave shape 0·50/2000 μs; (*d*) 310 kV crest voltage, wave shape 0·20/2000 μs; (*e*) 540 kV crest voltage, wave shape 0·50/2000 μs; (*f*) 700 kV crest voltage, wave shape 0·20/2000 μs; (*g*) 700 kV crest voltage, wave shape 0·50/2000 μs.

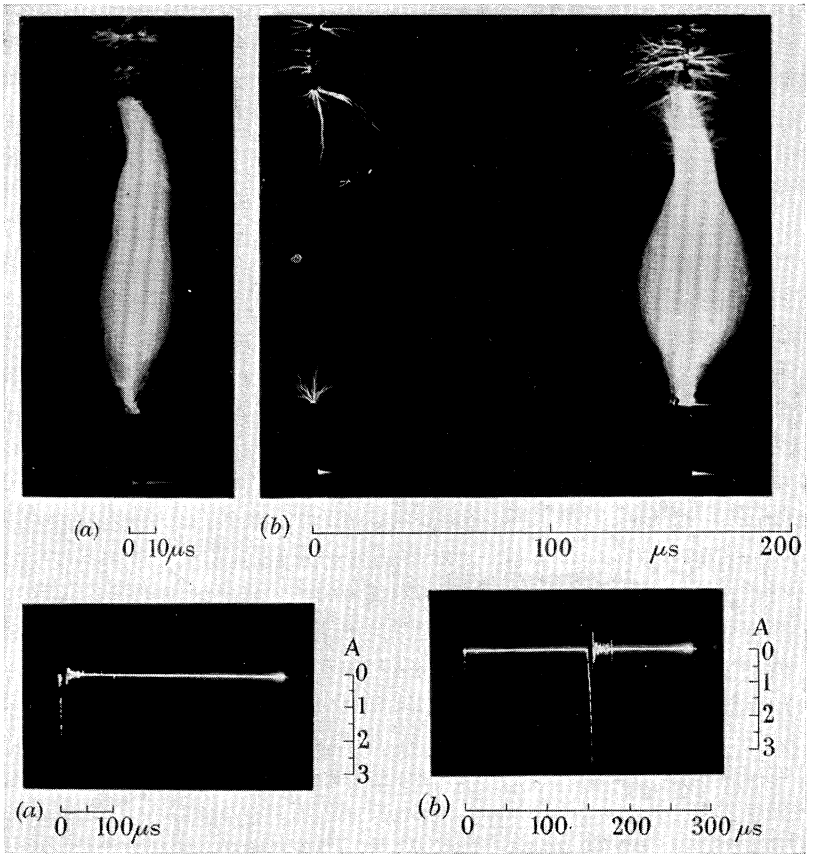

FIGURE 5. Time-resolved photographs of arrested breakdown in a 60 cm rod/rod gap for 440 kV crest voltage, wave shape 0·50/2000 μs.

(*Facing p.* 216)

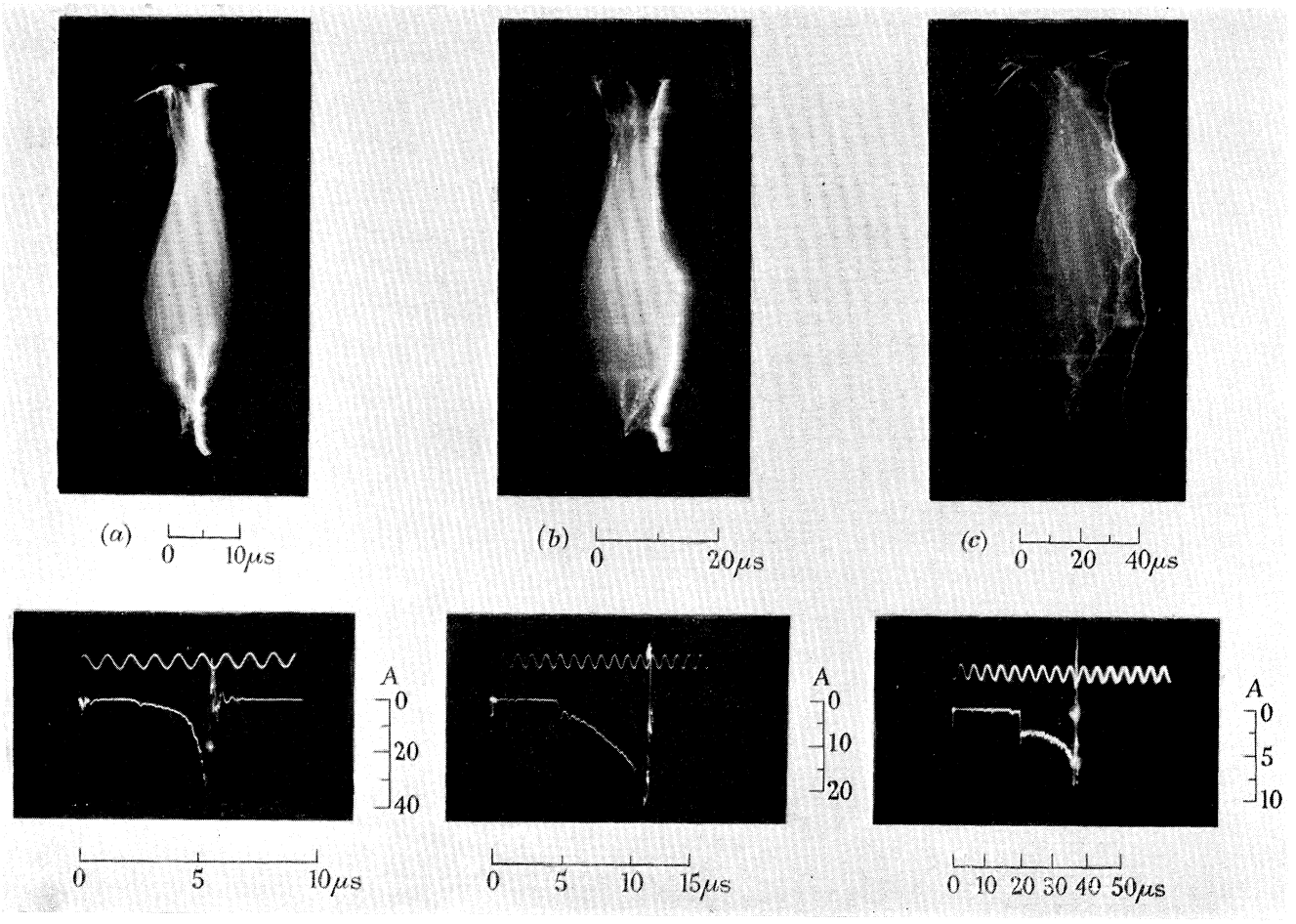

FIGURE 6. Time-resolved photographs of breakdown in a 106·7 cm rod/rod gap with increasing series resistance: (*a*) 790 kV crest voltage, added series resistance = 0 Ω; (*b*) 890 kV crest voltage, added series resistance = 20·5 kΩ; (*c*) 940 kV crest voltage, added series resistance = 200 kΩ.

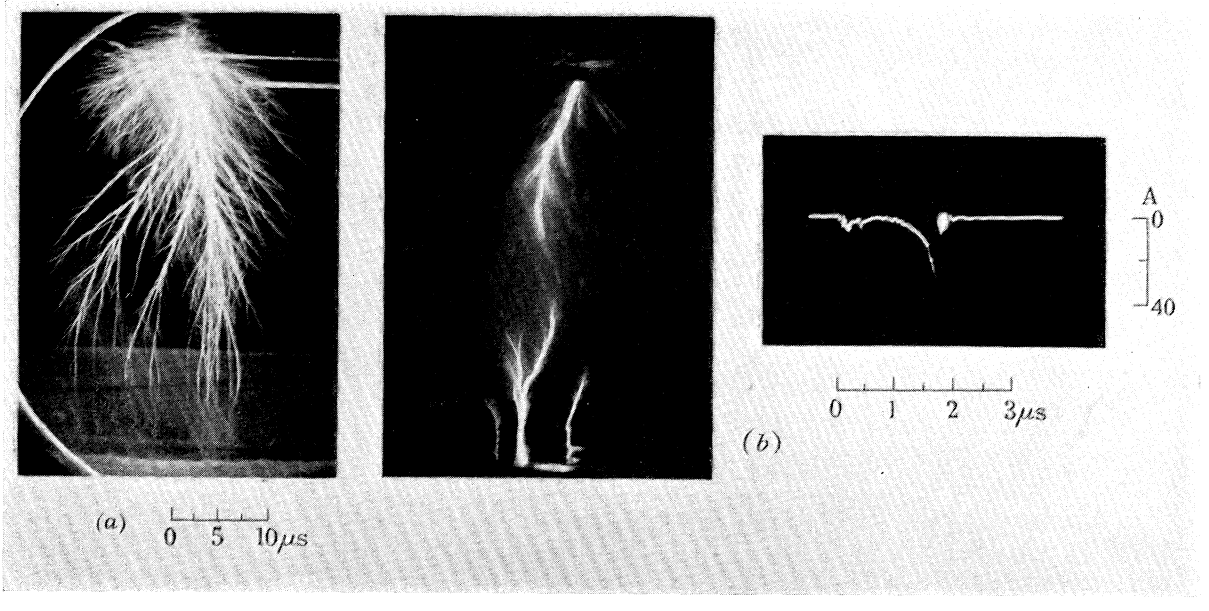

FIGURE 12. Time-resolved photographs of arrested breakdown in a 92 cm rod/plane gap for 1 MV crest voltage; wave shape 0·50/2000 μs.

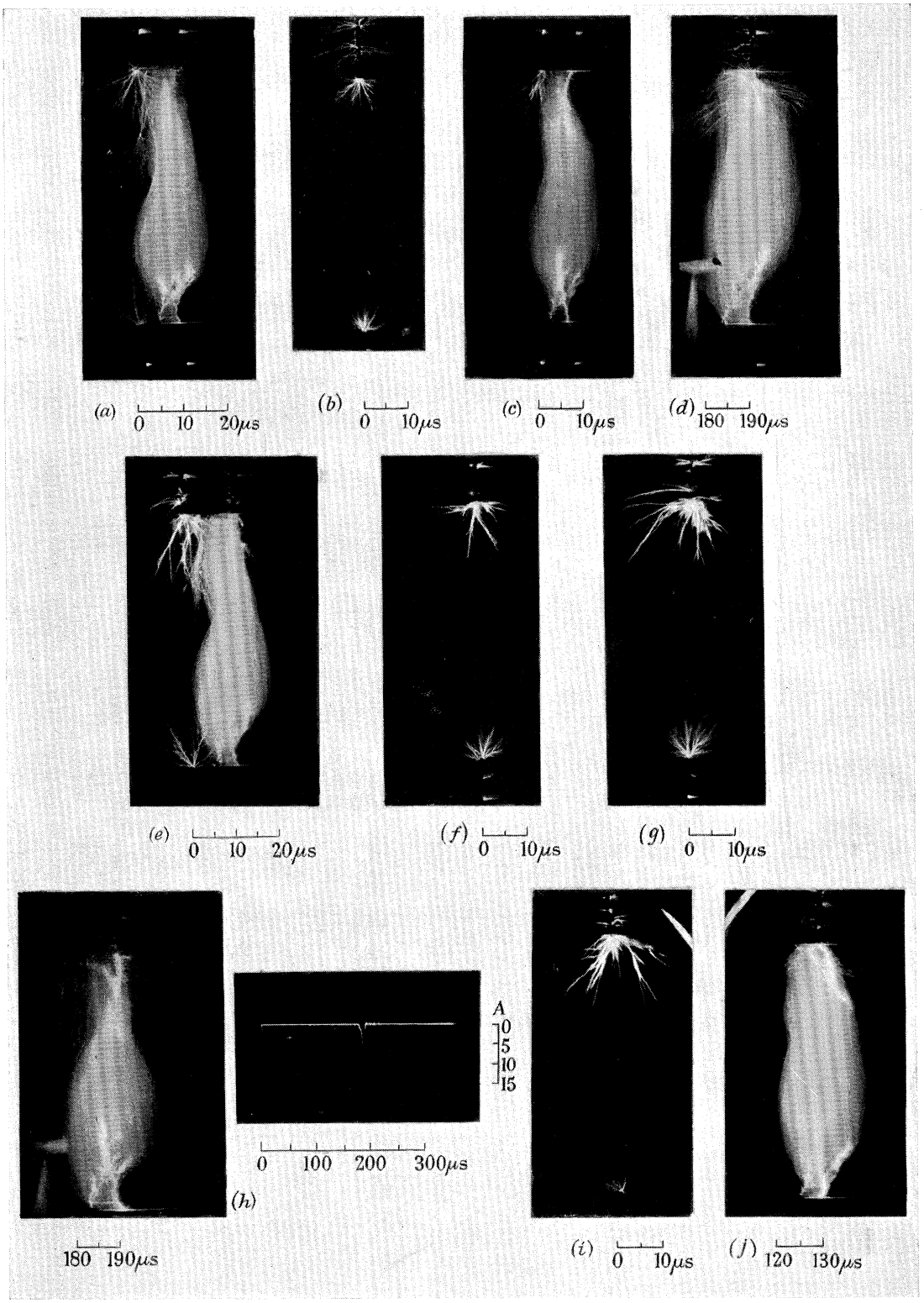

FIGURE 9. Time-resolved photographs of arrested breakdown in a 76·2 cm rod/rod gap with impulses of various wave front for 530 kV crest voltage. Wave shape: (*a*) 0·20/2000 μs; (*b*) 0·35/2000 μs; (*c*) 0·50/2000 μs; (*d*) 0·50/2000 μs; (*e*) 0·65/2000 μs; (*f*) 0·90/2000 μs; (*g*) 1·35/2000 μs; (*h*) 1·35/2000 μs; (*i*) 1·95/2000 μs; (*j*) 1·95/2000 μs.

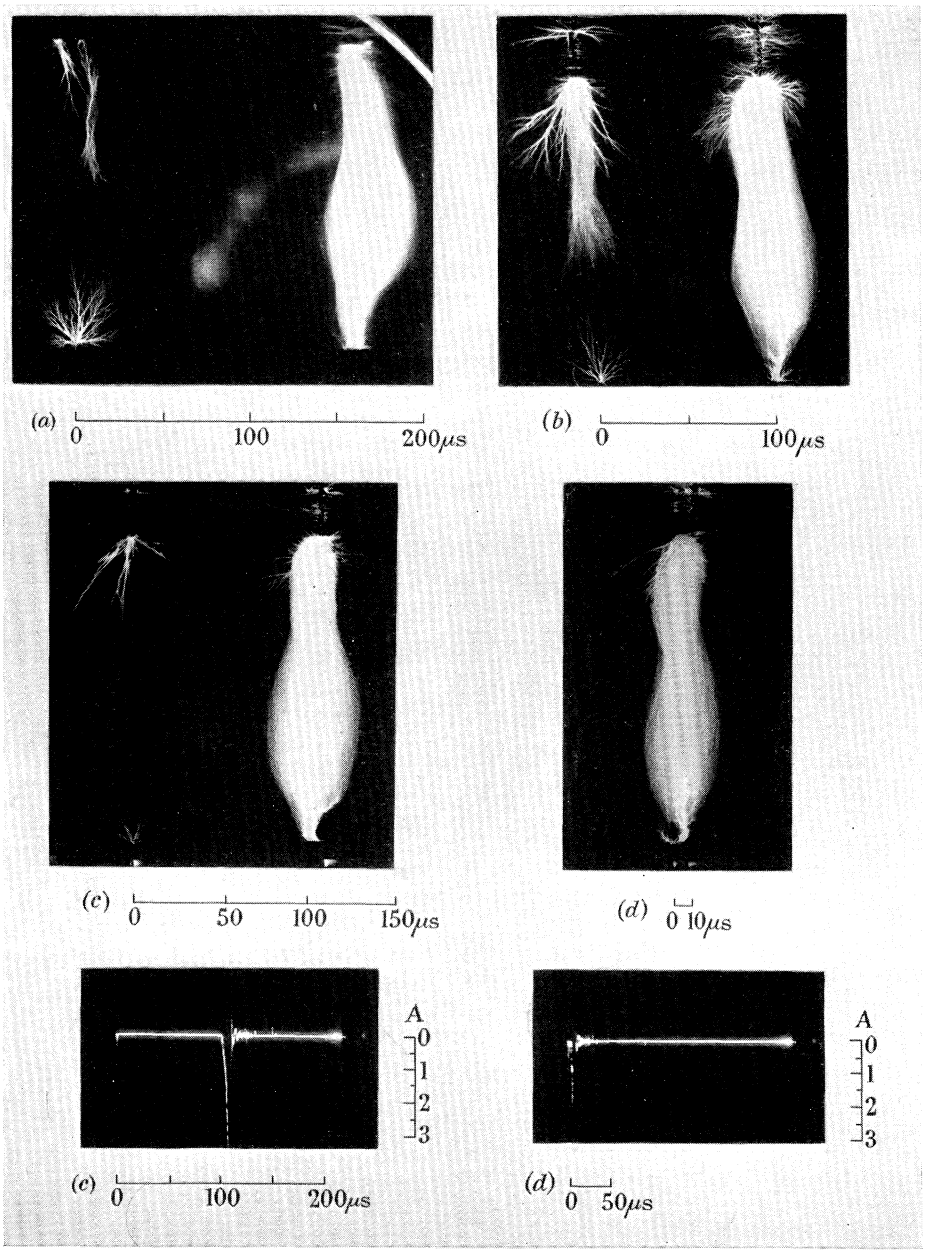

FIGURE 14. Time-resolved photographs of arrested breakdown in an 80 cm rod/rod gap for 550 kV crest voltage; wave shape 0·50/2000 μs.

PHILOSOPHICAL TRANSACTIONS OF THE ROYAL SOCIETY A MATHEMATICAL, PHYSICAL & ENGINEERING SCIENCES

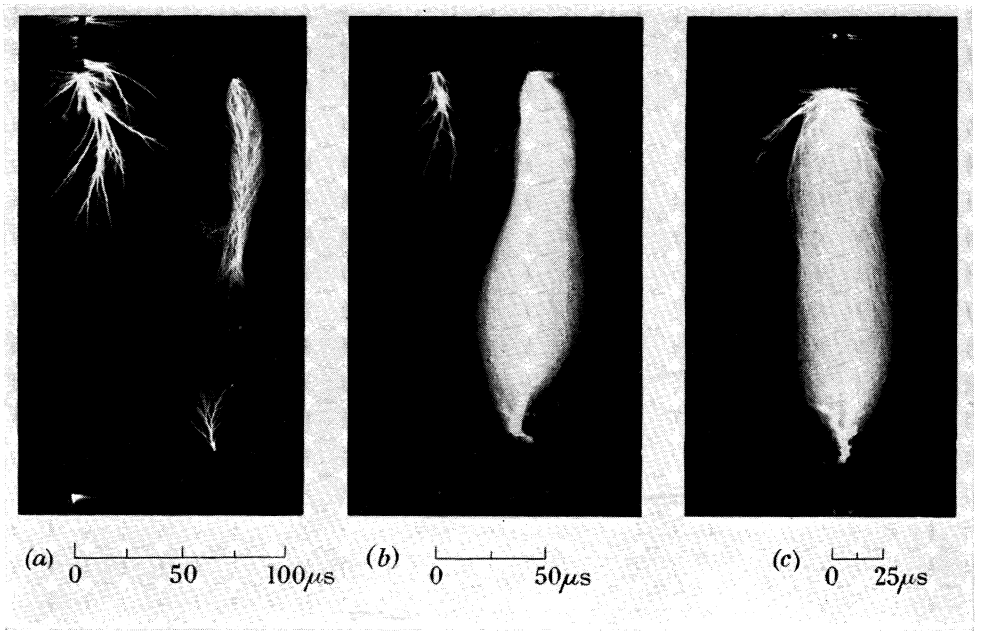

FIGURE 15. Time-resolved photographs of arrested breakdown in an 80 cm rod/6·25 cm diameter sphere gap for 570 kV crest voltage; wave shape 0·50/2000 μs.

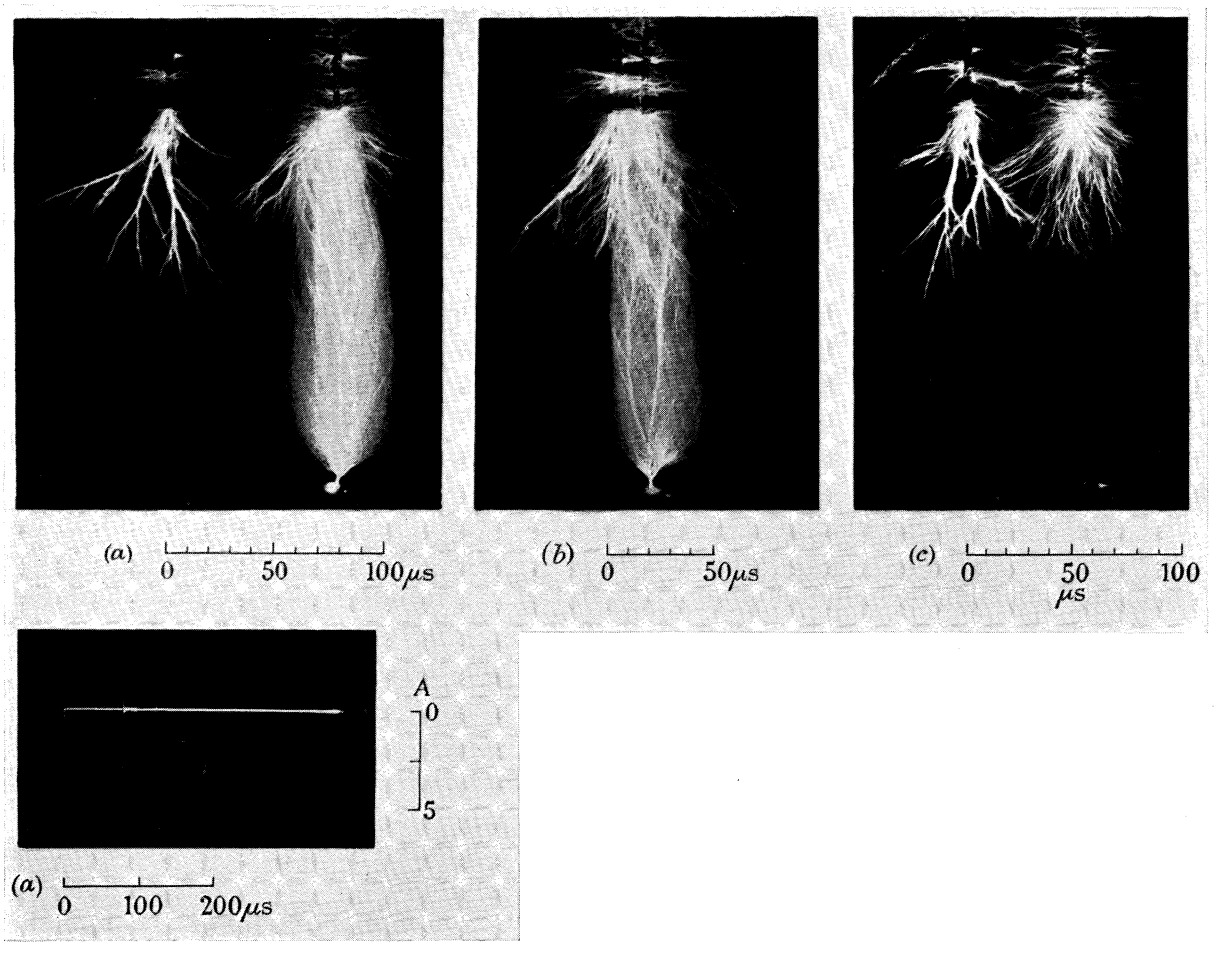

FIGURE 16. Time-resolved photographs of arrested breakdown in an 80 cm rod/12·5 cm diameter sphere gap for 710 kV crest voltage; wave shape 0·50/2000 μs.

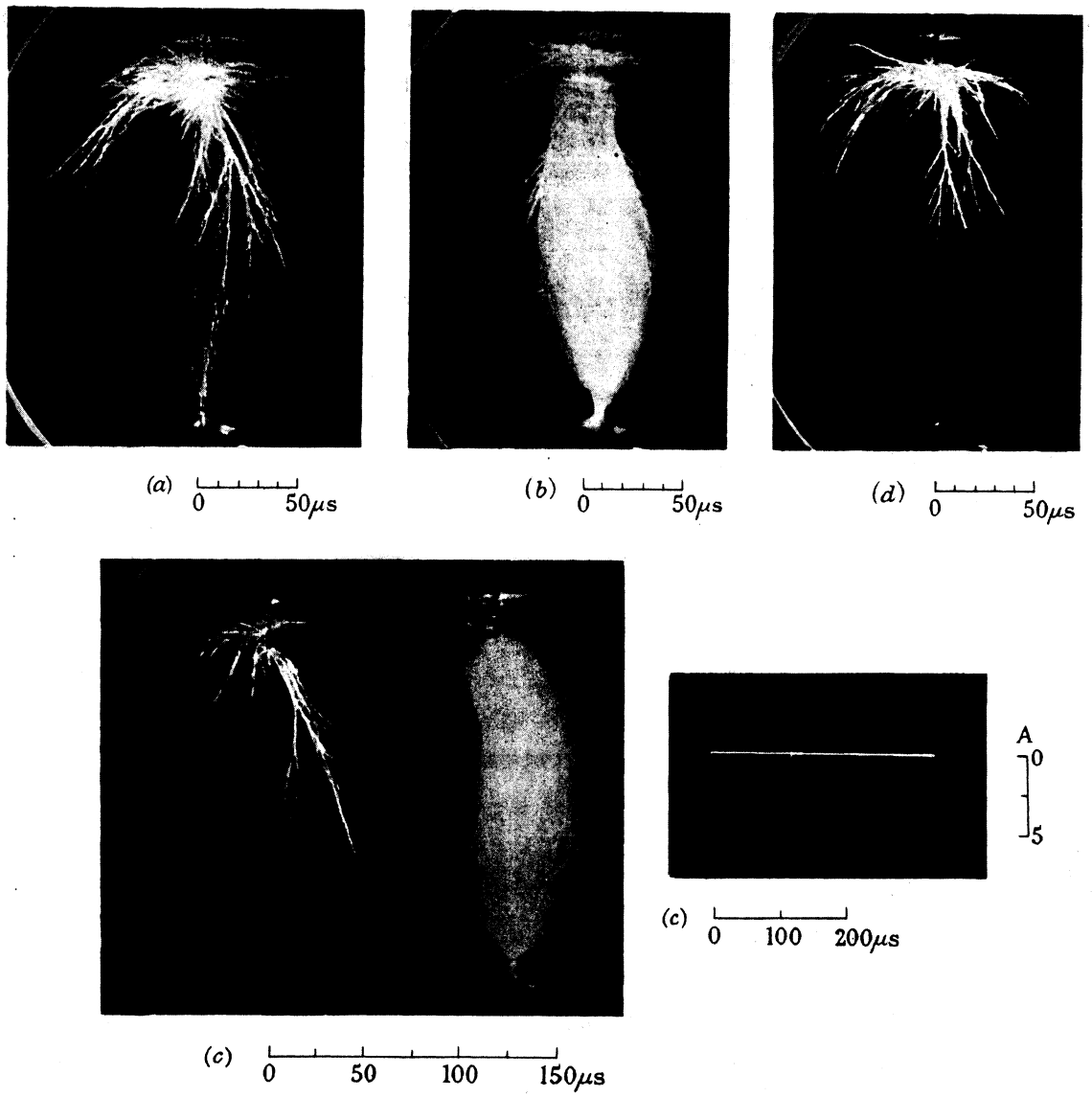

FIGURE 17. Time-resolved photographs of arrested breakdown in an 80 cm rod/25 cm diameter sphere gap for 860 kV crest voltage; wave shape 0·50/2000 μs.

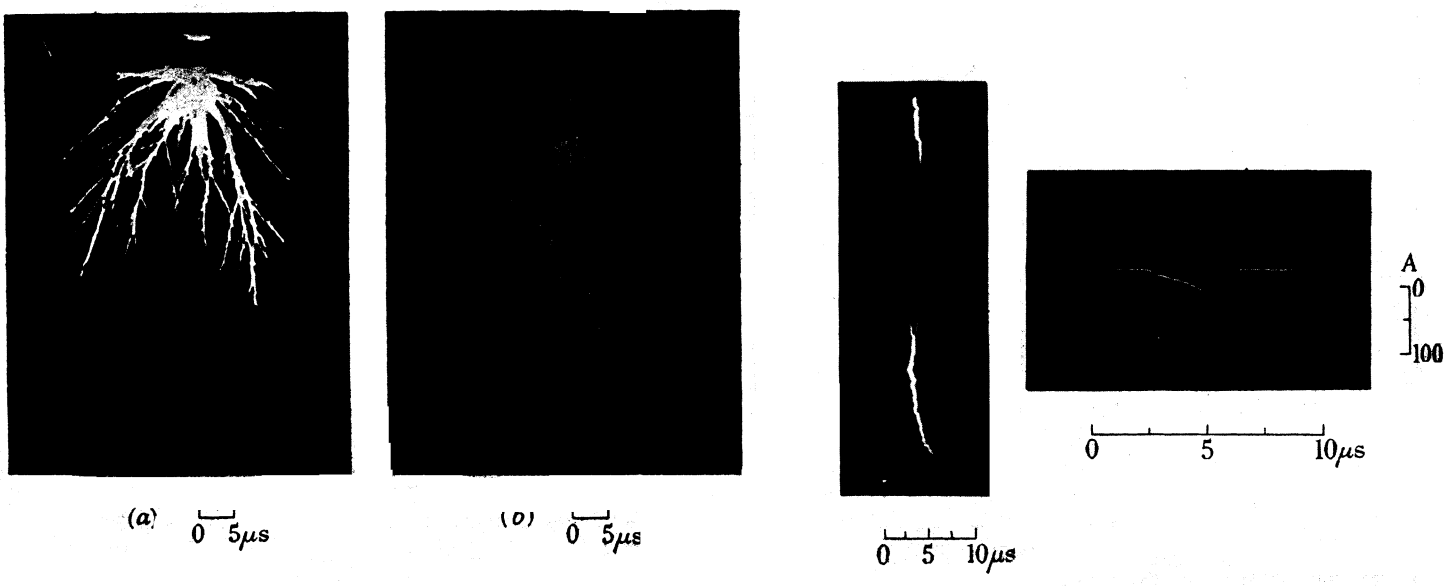

URE 18. Time-resolved photographs of arrested breakdown in an 80 cm rod/75 cm iameter sphere gap; wave shape 0·50/2000 μs; (*a*) 830 kV crest voltage, (*b*) 900 kV rest voltage.

FIGURE 19. Time-resolved photograph of arrested breakdown in a ' diameter sphere/rod gap for 860 kV crest voltage; gap spacing 106· wave shape 0·50/2000 μs.

Tests using two impulse wave shapes of identical crest values and wave fronts, but of wave tail 34 and 2000 μs respectively, showed that the sole effect of a shorter wave tail was to exclude sparks of long time lag without affecting the frequency of short-lag breakdowns.

The greatest contrast between impulses of differing polarity was produced at the larger gap spacings. Negative impulses were found to produce breakdowns of long time lag and

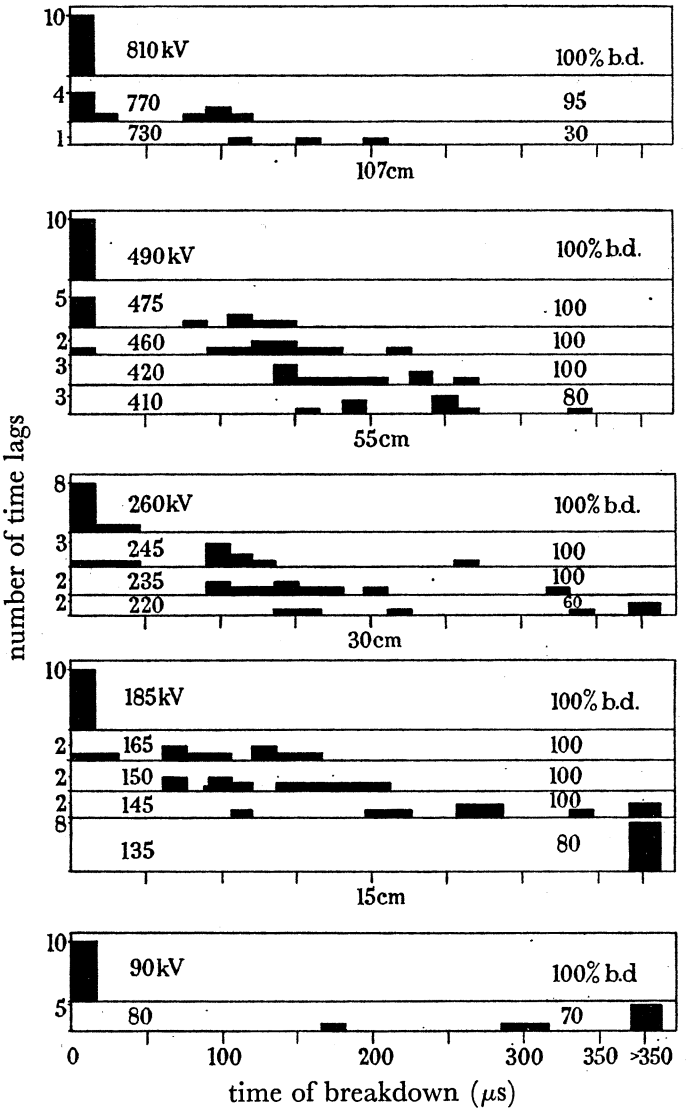

FIGURE 4. Time-lag histograms for rod/rod gaps subjected to 0·50/2000 μs impulses at increasing voltage levels.

the characteristic twin-maximum histogram for all gap lengths investigated (a maximum of 122 cm), as compared with the disappearance of long time lags with positive impulses for rod/rod gaps exceeding 70 cm.

The f/1·0 streak camera was used, with a mirror speed of 9000 rev/min producing an image speed of 0·105 mm/μs, to record the breakdown of a 60 cm rod/rod gap with a 0·50/2000 μs impulse of crest voltage 440 kV. Figures 5 (a) and 5 (b), plate 10, show two of the discharges photographed, the breakdown in each case being arrested before

completion in the manner described in part I, in order to prevent fogging of the record. The time lag for discharge (*a*) was 5·8 μs, and for (*b*) 156 μs. It can be seen from record (*b*) that, following the corona discharge from both cathode and earthed anode near time zero, no further visible discharge occurred until 151 μs; the leader process was then initiated and a time of merely 5 μs was required to complete the breakdown of the gap. Thus throughout the dead-time of, in this case, 151 μs, no discharge occurred despite the maintenance of potential difference across the gap.

An increase in the time lag may also be brought about by the use of a resistance in series with the gap; this increase, however, is due to the longer formative time lag effected by a reduction of the potential difference across the gap. Figure 6, plate 11, shows time-resolved photographs (obtained with a lens transparent to ultraviolet of aperture *f*/2·3) of breakdown in a 106·7 cm (42 in.) rod/rod gap with 0·50/2000 μs impulses. The series resistance and impulse voltages are in record (*a*) 0 Ω, 790 kV, (*b*) 20·5 Ω, 890 kV and (*c*) 200 kΩ, 940 kV. The limitation of current in (*b*) and (*c*) was such that no arrest of the discharge before sparkover was necessary. As found by Allibone & Meek (1938), a periodic interruption of the leader stage may be brought about by the high series resistance.

(ii) *Variation of breakdown probability with time*

The time-lag studies indicated a changing probability of breakdown during the application of an impulse voltage, the magnitude and location of the two maxima depending on the experimental conditions. In order to confirm this conclusion, the superimposed impulse technique described in §2 was employed.

Figure 7 (*a*) shows the result of applying a further negative voltage of 55 kV to a 56 cm rod/rod gap already being subjected to a negative impulse of 405 kV crest (1·5/2000 μs wave). Such an impulse, without added voltage, caused a low percentage breakdown, these breakdowns being of long time lag. The efficiency of the added voltage in causing breakdown of the gap varied with its time of application, the probability of breakdown being at a minimum at a time of 15 μs following the application of the main impulse.

A superimposed voltage of this magnitude was too large to examine the variation of probability of breakdown at times longer than 80 μs. A smaller impulse of 28 kV was used, and this was added to the generator output at times up to 600 μs, as shown in figure 7 (*b*). For these longer times of superimposition the random scatter in the time of appearance of the step impulse was rather large ($\pm$25 μs), owing to the nature of the pulse-forming circuit. This lack of resolution was not, however, a serious difficulty. The curves obtained were of good reproducibility. A steep increase in the percentage breakdown until a time of 150 μs on the impulse wave tail was followed by a shallow minimum and a further, slightly higher maximum at 350 μs. The decrease in breakdown probability at longer times was due to the decay of the primary impulse voltage.

The form of figures 7 (*a*) and (*b*) thus amply confirms the time-lag histograms of figure 4.

(iii) *The effect of impulse wave front on breakdown voltages and time lags*

A 76·2 cm (30 in.) gap was subjected to impulses of fixed crest voltage but of varied rise-time. Figure 8 illustrates the variation of percentage breakdown with wave front at a

crest voltage of 530 kV. Although complex, the form of the curve was found to be fully reproducible. The breakdown probability was found to be dependent upon the wave front over a larger wave front range than for positive impulses, and showed a cyclic variation. As an example of the resulting effect upon breakdown voltage, a change of

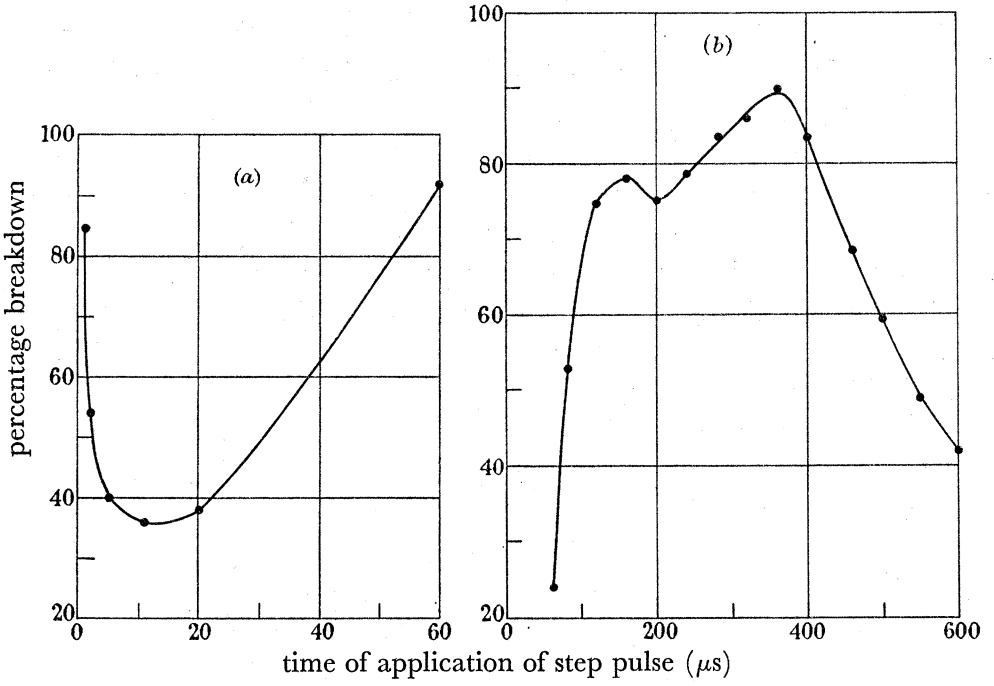

FIGURE 7. Variation with time of the probability of breakdown of a 56 cm rod/rod gap. (*a*) Main impulse crest voltage 405 kV, added voltage 55 kV; (*b*) main impulse crest voltage 405 kV, added voltage 28 kV.

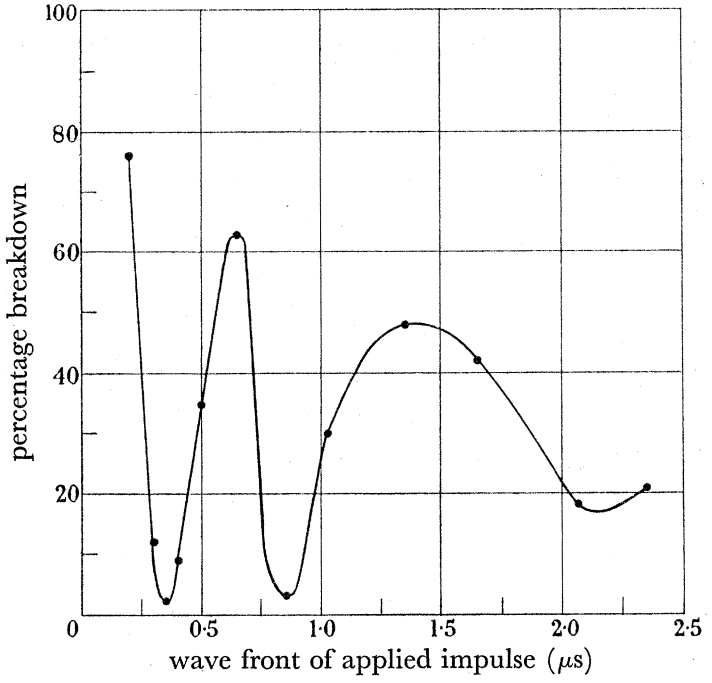

FIGURE 8. Effect of wave front on the breakdown probability of a 76·2 cm rod/rod gap for 530 kV.

impulse wave front from 0·65 to 0·42 μs necessitated an increase in crest voltage from 530 to 570 kV to maintain the percentage breakdown.

The first minimum (at 0·35 μs wave front) was found to be that retained most persistently with increasing voltage.

Time-lag histograms recorded during these observations also showed a consistent variation with wave front. Breakdowns for wave fronts less than 0·35 μs were almost wholly of short time lag. Few short time lags were found at longer wave fronts at 530 kV crest, the oscillatory variation in percentage breakdown being caused by an oscillation of the mean time value of the long-lag distribution. With a crest voltage of 540 kV a periodic variation with wave front in the number of short time lags then contributed to the fluctuation in percentage breakdown, but the oscillation of the long time lags was still evident. The ratio of short time lags to long was greater at the second maximum (0·65 μs wave front) than at the third (1·40 μs). This ratio increased at higher voltages.

Parallel experiments were also carried out in which the cathode was illuminated by ultra-violet radiation from a mercury arc quartz lamp, the arc image being focused on the electrode by a front-aluminized concave mirror. Generally ultra-violet irradiation was shown to increase percentage breakdown; invariably, however, the number of short time-lag sparkovers was fewer than in the non-irradiated case.

The discharge in the 76·2 cm rod/rod gap for an impulse crest voltage of 530 kV was photographed with the time-resolving camera. The image speed on the film was 0·31 mm/μs throughout. Figure 9, plate 12, shows the types of discharge obtained for various impulse wave fronts. Detailed description of these photographs will be found in Appendix II.

By means of an arrangement to reduce the inductance of the impulse generator described in part I, negative impulses of wave fronts down to 0·06 μs could be applied to the gap. Figure 10 shows the breakdown voltages measured for the three gap lengths 30, 52·5 and 70 cm.

The outstanding feature of these data was that for fast wave-front impulses the breakdown voltage was lower for negative impulses than for positive impulses. This was due to a fairly smooth decrease of 20 to 30% in the negative breakdown voltage with decreasing wave-front duration. The intersection of the positive and negative curves occurred at about 0·2 μs wave-front impulses for the larger gap spacings.

A further feature of figure 10 is the large overvoltage sometimes required to cause 50% short-lag breakdown over that producing 50% breakdown. For negative impulses the difference was greatest at the slower wave fronts; for positive impulses the maximum difference was in the intermediate wave-front range 0·1 to 0·3 μs.

For each wave front and gap distance in figure 10, a series of time-lag histograms were obtained for a range of voltages between the 0% breakdown and 100% short-lag breakdown levels. The general form of the distributions was similar to those of figure 4.

(*c*) *Rod/plane gaps*

The applied potentials causing 50% breakdown of rod/plane gaps were found for negative impulses of wave shape 0·20/2000 and 0·50/2000 μs. The results are presented in figure 11, together with results published by Allibone, Hawley & Perry (1934), Bellaschi & Teague (1934) and Gorev, Zalesky & Riabov (1948). There is good agreement between

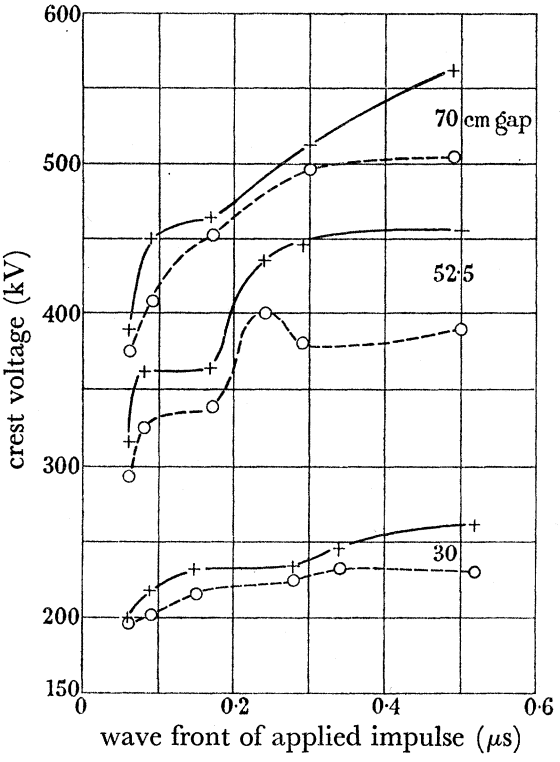

FIGURE 10. Variation of rod/rod gap breakdown voltages with impulse wave front. +, Points for 50 % breakdown after short time lag; ○, points for 50 % breakdown.

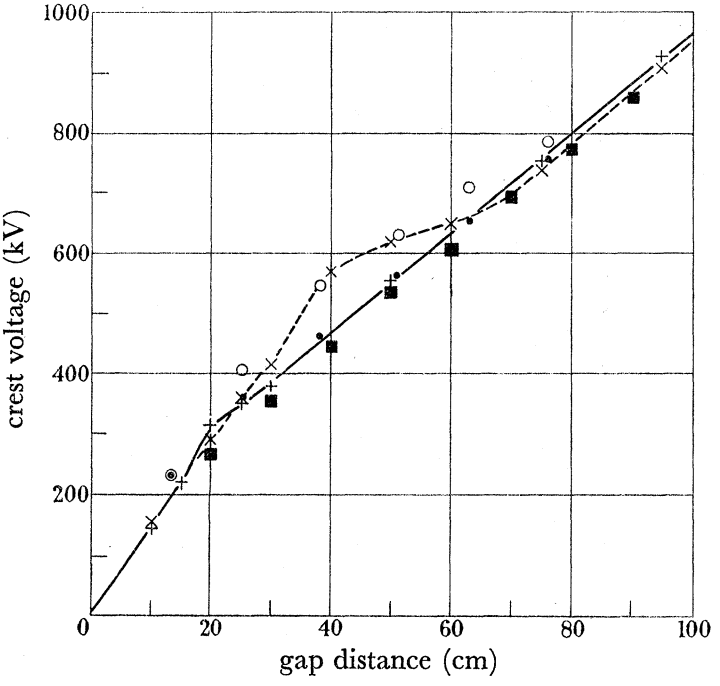

FIGURE 11. Breakdown voltages for rod/plane gaps, +, ×, present experiments, wave shape, 0·50/2000 μs (+), 0·20/2000 μs (×); ○, ●, Allibone *et al.* (1934), 1/580 μs (○), 1/50 μs (●); ▪, Bellaschi & Teague (1934), 1·50/40 μs.

PHILOSOPHICAL TRANSACTIONS OF THE ROYAL SOCIETY A MATHEMATICAL, PHYSICAL & ENGINEERING SCIENCES

the present results for a 0·50/2000 μs impulse and the 1·0/50 μs used by the previous workers. The work also confirms that whereas the positive rod/plane gap has a lower breakdown strength than the rod/rod gap, for negative impulses the rod/plane gap is considerably more difficult to break down than the rod/rod gap.

An interesting wave-front effect was found with gaps in the range 25 to 60 cm. Whereas at all other gap lengths the impulse wave front had little effect upon the breakdown probability, impulses of 0·20 μs wave front were distinctly less successful than those of 0·50 μs wave front in causing breakdown of gaps in the range quoted. The effect was greatest for a 40 cm gap, where with a 0·20 μs wave front a crest voltage of 570 kV was needed to produce 50% breakdown, compared with a voltage of 455 kV at 0·50 μs wave front. It is to be noted that this effect was the opposite of that found with the rod/rod gap, where the general trend was a decrease of breakdown strength with increasing rate of potential rise of the impulse. This result also suggested an explanation of the anomaly described in the early work of Allibone *et al.* (1934), where the increase of the impulse wave tail from 50 to 580 μs led to a similar increase in the breakdown strength of a rod/plane gap. The wave tail of the impulse was then controlled by a resistor across the output; removal of this resistor to extend the duration of the impulse wave tail may also have had the effect of increasing the rate of rise of the impulse wave front and so producing the effect described here.

An examination of the time lag to breakdown of negative rod/plane discharges showed that no long time lags occurred for any gap length which was examined. This was in direct contrast with the behaviour of the rod/rod gap, where the twin-maximum histogram was found for all gap spacings. It also differed from the behaviour with positive impulses, where breakdowns of long time lag were found over the same gap range for both rod/rod and rod/plane electrodes. The time to breakdown of negative impulse rod/plane discharges was extremely short, usually lying between 2 and 3 μs as found by Allibone *et al.* If breakdown failed to take place within this time, therefore, there was no likelihood of breakdown occurring during the remainder of the long-duration potential wave tail.

Figure 12, plate 11, gives examples of the breakdown of a rod/plane gap of electrode separation 92 cm with a 0·50/2000 μs impulse of 1 MV crest. It was invariably found that prior to breakdown the negative corona channels traversed the gap, as in record (*a*), which shows a discharge arrested before the growth of the leader channels. The anode leader was initiated at the point of contact of one or more of these channels with the plane. The high rate of breakdown made detailed time-analysis difficult, but it appeared that the onset of the leader was coincident at each electrode. The mean velocity of the leaders was 3×10^7 cm/s. The luminosity of the leaders was so great as to cause fogging in the $f/1{\cdot}0$ camera. Figure 12 (*b*) is a stationary record obtained with an $f/2{\cdot}5$ glass lens.

(*d*) *Rod/sphere gaps*

The great difference between the breakdown voltages of rod/rod and rod/plane electrode systems suggested that the examination of intermediate configurations would be of interest. For this purpose the gap length was fixed at 80 cm, the impulse wave shape was 0·50/2000 μs, the rod electrode was of the usual hemispherically tipped form, and the anode was composed successively of spheres of diameter 6·25, 12·5, 25 and 75 cm. A graph of the 50% breakdown voltage plotted as a function of anode diameter is shown in figure 13.

The foremost features were the small change in breakdown voltage between the rod/rod and rod/6·25 cm sphere gaps compared with the larger change at greater anode diameters, and the higher breakdown voltage of the rod/25 cm sphere gap compared with the rod/plane gap (895 and 810 kV respectively). All anodes used were of good surface finish, the plane electrode was of aluminium, the 75 cm diameter sphere of copper and the smaller spheres of brass.

The time lag of rod/sphere discharges was also measured. Breakdowns of long time lag were found for anode diameters 6·25, 12·5 and 25 cm, but were absent with the 75 cm diameter sphere. The dead-time was longer than in rod/rod breakdown, the majority of time lags being greater than 350 μs. The number of long time lags observed was greatest with the 6·25 cm diameter anode where, at 100% breakdown, all discharges were of this type.

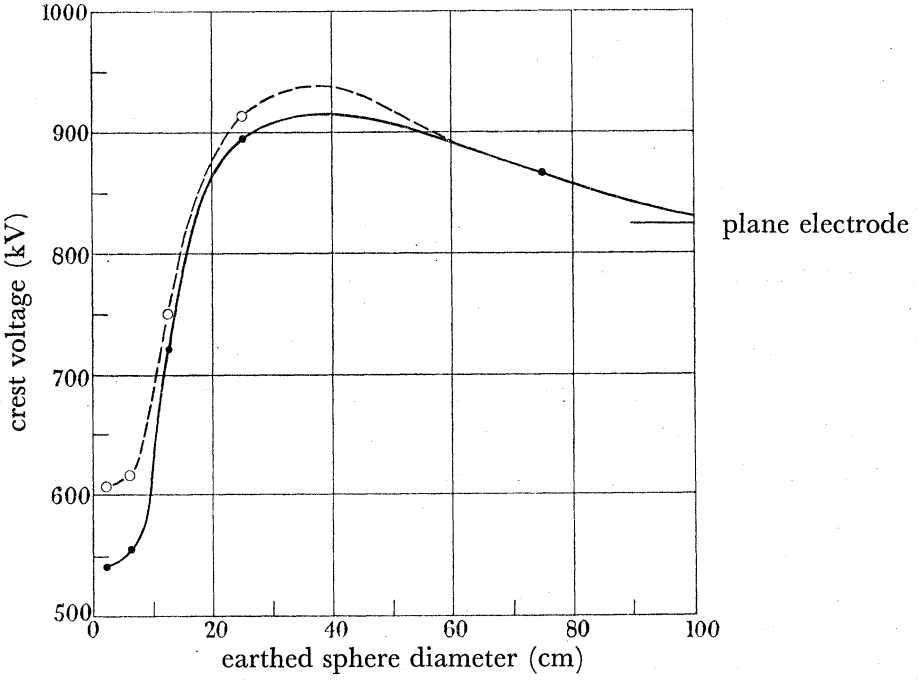

FIGURE 13. Variation of the breakdown voltage of an 80 cm rod/sphere gap with sphere diameter. ○, Points for 50 % breakdown after short time lag; •, points for 50 % breakdown.

The $f/1{\cdot}0$ camera was used to examine 80 cm rod/rod and rod/sphere systems at an image speed of 0·105 mm/μs, except for the 75 cm diameter anode where a speed of 0·315 mm/μs was used.

Figure 14, plate 13, shows discharges occurring for 550 kV in a rod/rod gap. Although, in most cases of rod/rod breakdown, the anode corona was found to coincide with the cathode corona near time zero, record (*a*) shows the anode corona to be delayed by 13 μs; it was accompanied by a further cathode discharge and the formation of mid-gap streamers. This was followed by breakdown after a total time of 170 μs. The mid-gap discharge could also be formed when the anode corona had no apparent delay in initiation, as in (*b*); the breakdown time was here 100 μs. The more usual discharge form was as in (*c*), the time lag being 109 μs. The cathode and anode corona extent was 28 and 11 cm respectively. A typical breakdown of short time lag (8·6 μs), which also occurred at 550 kV, is shown in (*d*).

The photographs of figure 15, plate 14, are of discharges in a rod/6·25 cm sphere gap at 570 kV. With this arrangement the onset of the anode discharge was frequently delayed, and it was more often accompanied by the discharge in the cathode half of the gap. In record (*a*) this delay was 69 μs, and it was followed by sparkover in 350 μs which, with the mirror speed used, was too long to be recorded. In (*b*) a discharge of 49 μs time lag was initiated by such an anode discharge. When the anode discharge occurred synchronously with the negative corona, a breakdown of short time lag often resulted ((*c*), 7 μs).

Rod/12·5 cm sphere discharges are shown in figure 16, plate 14. In this case no anode discharge classifiable as a corona discharge was found. A straight stem of 1·5 cm length was formed, which developed branches and assumed the self-propagating character of a leader stroke. Record (*a*) indicates the development of such an anode discharge after 77 μs. Long corona channels spanned the gap between the anode leader and the cathode, accompanied by the usual uniform glow in the inter-leader space. The negative leader was also formed at this stage. The initial negative corona was extensive under these conditions, traversing half the gap distance. Record (*b*) is a discharge of short time lag (13·3 μs), which was otherwise similar in structure to record (*a*). The extent of the space charge injected into the cathode region by the initial corona discharge is shown by record (*c*), in which case the impulse potential was removed after 53 μs without any leader having been formed. At the instant of removal a second corona discharge occurred at the rod; this was of a form usually associated with the positive impulse corona, and so indicated the presence of appreciable negative space charge in the vicinity of the cathode.

Figure 17, plate 15, shows the various types of discharges obtained in the rod/25 cm sphere configuration at 860 kV crest voltage. Record (*a*) revealed that the negative corona was able to traverse 69 cm of the 80 cm gap. The discharge was arrested after a voltage application of 1·0 μs. The straight discharge shafts from the anode were 3·5 cm in length, and the cathode-directed branches link with the downcoming negative corona channels. Record (*b*), which was a discharge having developed for 1·6 μs before removal of the voltage, shows the growth of the anode and cathode leaders and the uniform glow. Where the negative corona channels did not approach the anode so closely, a breakdown of long time lag could result (record (*c*), time lag 116 μs). As in the rod/12·5 cm sphere gap, the anode leader was then accompanied by corona channels crossing the gap. The discharge in record (*d*) failed to result in breakdown of the gap. Several such records showed corona streamers less extensive than those preceding sparkover.

The no-breakdown case of a rod/75 cm sphere gap recorded in figure 18 (*a*), plate 15, at 835 kV shows no anode discharge despite the approach of the negative corona channels to within 7 cm of the earthed sphere. Record (*b*) leaves no doubt that in the breakdown of rod/75 cm sphere gaps the negative corona channels completely bridged the gap. This discharge took place at 900 kV and was arrested after 1·2 μs.

(*e*) *Sphere/rod gaps*

The photograph of figure 19, plate 15, was obtained with a glass lens of aperture *f*/2·5 and focal length 7 in., with an image speed on the film of 0·31 mm/μs, in order to record the discharge with the maximum time-resolution available. The high-tension cathode was a 75 cm diameter sphere, opposed by a rod electrode 106·7 cm distant. The crest voltage

was 860 kV. It is seen that the positive leader began at 2·25 μs, and had progressed some 30 cm before the negative leader was initiated. The mean negative leader velocity was, however, 5×10^{-7} cm/s compared with 1×10^{7} cm/s for the positive leader. The discharge was suppressed at 5·7 μs.

4. Discussion

(*a*) *The impulse wave front and negative corona*

Even at the onset potential the negative corona displayed distinct differences from the positive corona. The onset potential was itself 17% lower than under positive impulses, and the discharge was of glow rather than filamentary structure and of 0·8 cm extent compared with the 4 cm of the anode discharge. Since the initiation of the discharge is known to depend upon the presence of atmospheric ionization (Park & Cones 1956), it is difficult to account for the polarity difference of onset potential or the low electric field required to produce a negligible statistical time lag (Loeb (1935) has stated that $E/p = 90$ provides the criterion for detachment). It is possible that the onset of the negative corona is aided by secondary electrons in a Townsend process, and that the development of the avalanche in a falling field is less likely to produce the space charge concentration that is necessary to lead to the corona channel. Such channels were, however, observed at higher crest voltages, and the importance of the rate of potential rise at the electrode was immediately apparent.

For crest voltages up to 300 kV, wave fronts of both 0·20 μs and 0·50 μs produced solely forward-developing channels; those developing on the 0·20 μs wave front were more extensive. A similar effect was observed for positive impulses, and the probable explanation is again that the faster wave front is able to maintain a sufficient electric field to continue propagation of the channels despite the self-quenching action of the corona space charge.

At voltages in the range 300 to 700 kV, while the 0·20 μs wave front continued to produce a large hemispherical envelope of channels developing from the cathode, the 0·50 μs wave front caused a new form of breakdown. These were extensive channels which appeared to form at the periphery of the small hemispherical corona. As deduced from the branched structure, propagation takes place towards both cathode and anode. It is reasonable to conclude that the early self-extinction of the primary corona discharge enables the potential gradient to attain a sufficient level to release further electrons, and so lead to the formation of the retrograde streamers.

At voltages in excess of 700 kV the retrograde streamers were found even with the faster wave front; it is possible that with a rate of voltage rise in excess of $3{\cdot}5 \times 10^{6}$ V/μs the forward-growing discharge cannot sufficiently moderate the electric gradient and so prevent the formation of the retrograde streamers.

The streak photographs of figure 9 show the variation of negative corona for wave fronts slower than 0·50 μs. The development of the retrograde streamers is again similar at 0·65 μs, but at 0·90 μs wave front their overall length is somewhat less. As surmised earlier, this may be due to a self-quenching action which operates due to the slowly rising potential gradient. The extent of the streamers, however, is observed to increase when the wavefront is further retarded to 1·35 μs. In this case the first phase of the corona cannot be detected on the photographs. The early moderation of the potential gradient may now

PHILOSOPHICAL TRANSACTIONS OF THE ROYAL SOCIETY A MATHEMATICAL, PHYSICAL & ENGINEERING SCIENCES

be so minimized that the retrograde streamers may develop under more favourable conditions than at the 0·90 μs wave front. The observation that, for the slowest wave front employed of 1·95 μs, many retrograde streamers initiate 4 to 13 cm from the electrode is probably due to a second generation of such streamers arising near the termination of the first.

(*b*) *Influence of impulse characteristics and gap geometry on breakdown voltages and time lags*

The primary interest arising from the results presented in both parts of this paper is whether an explanation can be given for the effects produced by changes of the polarity and wave shape of the applied potential and of the electrode configuration. These effects may be summarized as follows:

(1) Whereas the breakdown voltage of rod/rod gaps for standard wave forms is greater for negative polarity than positive, the reverse is the case for impulse wave fronts faster than 0·20 μs.

(2) For negative impulses the potential difference required for the breakdown of rod/plane gaps is 50% greater than of rod/rod gaps; with positive impulses the rod/plane gap breakdown voltage lies 15% below the rod/rod level.

(3) An increase in the rate of potential rise of the negative impulse wave front is found to reduce the probability of breakdown of rod/plane gaps in the range 25 to 60 cm. This effect is the reverse of the result found for rod/rod gaps. No variation of breakdown voltage with wave front is evident for rod/plane gaps with positive impulses.

(4) In rod/sphere gaps with negative impulse potentials the breakdown voltage is not sensitive to anode radius for small radii; for intermediate anode size the breakdown voltage increases sharply with increasing anode radius, but a fall is observed for large radii. For positive impulses a steady decrease of breakdown voltage is observed with increasing sphere radius.

(5) In sphere/rod gaps the breakdown voltage is less for negative impulses than for positive.

(6) Breakdowns of long time lag are found for the full range of rod/rod gaps investigated with negative impulses, while they are absent for gaps greater than 70 cm for positive impulses.

(7) No long-lag breakdowns occur in negative impulse rod/plane breakdown. Their probability of occurrence increases with decreasing anode radius. For positive impulses, on the other hand, the rod/plane gap exhibits time-lag characteristics similar to the rod/rod gap.

(8) While the time lag of negative impulse discharges which are uninterrupted by any dead-time decreases markedly with increasing anode radius, a slight increase occurs with positive impulses and increasing cathode radius.

The major conclusion to be drawn from the photographic evidence is that in the range of gap lengths which have been investigated, and to within the accuracy of time measurement available, the negative leader never forms before the positive leader, although the reverse is often the case. Even where the disparity between the applied electric gradient at the cathode and anode was greatest, namely in the rod/plane gap under negative impulses, the development of the leader channel appeared to be coincident at either

electrode. It is already well known that the negative leader velocity is generally slightly less than that of the positive leader. Allibone & Meek (1938) have ascribed this to the positive ion space-charge disposition near the head of the channel. It is reasonable to suggest, therefore, that it is the successful formation of the anode leader channel which constitutes the criterion for breakdown in any gap in the range described, whatever the form of the applied potential. Stekolnikov & Shkilev (1962) have recently shown that for rod/plane gaps of more than 100 cm, the negative leader channel does form before any discharge from the anode.

The magnitude of the electric gradient at the anode will depend not only upon the geometry of the anode, but also upon the effect produced by the space charge of the negative corona discharge. Since the form of the negative corona has been found to be sensitive to wave-front change, especially at high rates of potential rise, corresponding variations would be expected in the probability of breakdown. These will now be discussed for the various gap systems.

(*c*) *Rod/sphere and rod/plane breakdown*

In rod/sphere gaps under positive impulses, the decreasing breakdown voltage with increasing cathode radius was ascribed to the increase in the field near the positive rod electrode produced by the image of the positive corona in the cathode; that is to say, the presence of a physically large cathode reduced the quenching effect of the positive corona and so aided the formation of the positive leader at the rod.

With negative impulses, however, the onset of the final breakdown stage is not initiated at the rod but at the earthed electrode, so this argument will not be valid. Indeed an entirely different variation of breakdown voltage with anode radius has been shown in figure 13. The difference of 3% in breakdown strength between the rod/rod and rod/6·25 cm sphere gaps is perhaps surprisingly small, since the larger anode would have a much smaller electric field induced at its surface than would a rod. On the other hand, there are three factors which would tend to compensate for this effect. First, the anode discharge from a 6·25 cm spherical anode is usually delayed, by which time the induced field will have increased by virtue of charge separation in the negative corona. Secondly, in the case of a rod anode, the positive corona will almost certainly be initiated during the growth of the negative corona, and the inevitable self-quenching will moderate the size of the induced field. Thirdly, the gradient at the larger anode will be less divergent than that at a rod electrode, and any discharge which is initiated will be less liable to self-quenching.

At greater anode radii the situation must arise when the induced field is no longer sufficient to initiate an anode discharge without a large increase in the magnitude of the negative corona. A considerable increase in breakdown voltage is thus observed for the rod/12·5 cm sphere and rod/25 cm sphere arrangements. Furthermore, the electric field adjacent to the anode is so nearly uniform that self-quenching of the discharge is not possible. Then no anode corona stage is observed and the ionization is sufficiently vigorous to form a leader channel in a self-propagating condition.

For the 75 cm sphere and plane earthed anodes a reduction in the breakdown strength occurred. Now in this case the induced charge on the anode surface, produced by the

PHILOSOPHICAL TRANSACTIONS OF THE ROYAL SOCIETY A MATHEMATICAL, PHYSICAL & ENGINEERING SCIENCES

volume of space charge of the negative corona, is never sufficient to raise the anode field to breakdown proportions. The photographic evidence suggests that it is necessary for the negative corona channels to traverse the gap and make contact with the anode. This will presumably set up high local fields by virtue of the removal of electrons in the channels by conduction into the anode: the positive leader(s) seems invariably to develop along one or more of the negative corona channels. But the extent of development of the negative corona is governed by the minimum potential gradient in the space through which it propagates. This minimum gradient will, for a given applied voltage and gap spacing, be greater for larger anode radii, and thus the earthed electrode will be more easily attained.

The necessity, in gaps of less than 100 cm, for the cathode corona streamers to traverse the gap to cause breakdown when the anode is of large dimensions, immediately accounts for the high breakdown strength not only of rod/plane gaps under negative impulses but also of sphere/rod gaps under positive impulses. The presence of surrounding earthed objects which lower the cathode field gives the large high-tension anode versus earthed rod configuration a higher breakdown voltage than any other arrangement in which one electrode is a rod.

The time lag of gaps with a rod cathode varied inversely with the anode radius. This was due to the faster formation of the anode leader in the more uniform gradient near a large anode, and the high mean gradient necessary in the gap to produce the extensive corona phase.

The influence of wave front upon the breakdown voltage of rod/plane gaps, as demonstrated in figure 11, is consistent with the observed behaviour of the negative corona discharge.

The initiation of the retrograde streamers greatly increases the extent of the negative corona. Since in the rod/plane gap the negative corona must reach the anode for breakdown to result, the reason for the effect caused by the impulse wave front on the breakdown of rod/plane gaps in the voltage range 350 to 650 kV is now clear; it is in this range that the retrograde streamers are formed more easily with a wave front of 0·50 μs, which results in a lower breakdown strength with this wave shape.

If the corona streamers from a rod-cathode fail to reach the earthed plane, there is little possibility of further ionization within the impulse duration; the induced gradient at the anode can never increase sufficiently to cause breakdown despite the drift of negative ions towards it, and the extensive negative corona appears efficiently to moderate the cathode field. No breakdowns of long time lag were thus observed with negative rod/large anode gaps.

(*d*) *Rod/rod breakdown*

(i) *Polarity effects*

Since the formation of the positive leader is the necessary precursor to breakdown, the lower breakdown potential for impulses of slow wave front of the rod/rod gap when the impulse polarity is positive is understandable; the high gradient at the high-tension rod leads to intense ionization in the corona discharge, which constitutes a more favourable embryo for development of a leader channel than the weaker corona occurring at a grounded anode. Furthermore, a discharge will occur at the earthed electrode only if an initiatory electron is produced. When the earthed electrode is anode, the probable source of supply

is from negative ion detachment, which requires a high electric gradient. For an earthed cathode the need for such high fields is reduced by other sources of supply, e.g. electron release from the cathode surface by photon- or ion-bombardment. Thus for a given extent of high-tension corona growth, the discharge from the earthed electrode will be produced at larger gap lengths for a positive applied impulse.

With fast wave fronts, however, the corona extent increases rapidly with increasing rate of voltage rise. Thus a general trend towards a decrease in the negative breakdown voltage will result owing to an increase in the rapidly induced anode field. This will shortly be examined in more detail. In the positive impulse case this will be counteracted by the increase of masking anode space charge for a given applied field and other effects which have been fully discussed in part I.

(ii) *The statistics of rod/rod breakdown*

The probability of the value $x = r$ in a Poisson distribution of mean $x = m$ is given by

$$P(r) = \frac{m^r \, \mathrm{e}^{-m}}{r!}. \tag{1}$$

Thus if a set of points is distributed at random in an interval, the probability of n points lying in a subinterval of length l is

$$P(n, l) = \frac{(l/\sigma)^n \, \mathrm{e}^{-l/\sigma}}{n!}, \tag{2}$$

where σ is the mean interval between points.

Then the probability of at least one point falling in an interval l is

$$\sum_{n=1}^{\infty} P(n, l) = 1 - \mathrm{e}^{-l/\sigma}. \tag{3}$$

If σ is the mean statistical time lag of appearance of an electron, this analysis can be applied to the present problem. As discussed in part I, both theoretical considerations and the experimental work of Brago & Stekolnikov (1958) suggest that the mean value of σ, which may be regarded as the mean time to produce detachment from negative ions, will not vary rapidly with wave front except for very slow rates of voltage rise. The faster the wave front, therefore, the higher will be the accelerating potential gradient in which the freed electrons are available. Let us suppose that, for a given crest voltage, electrons appearing not earlier than some time $k_1\tau$ on the wave front create sufficient space charge in the negative corona phase to initiate breakdown at the earthed anode rod; here τ is the total duration of the wave front and k_1 some factor less than unity. From the self-quenching effect already described, electrons appearing before $k_1\tau$ but after, say, $k_2\tau$, produce a reduced corona burst ($k_1 < k_2$); a lower probability of breakdown will follow. Similarly, the appearance of retrograde streamers will give a higher breakdown probability in the statistical lag range $k_3\tau$ to $k_2\tau$. The self-quenching of these streamers is suggested to reduce the likelihood of breakdown for the wave front period $k_4\tau$ to $k_3\tau$, with a second increase in the negative corona magnitude from $k_5\tau$ to $k_4\tau$ resulting from the increasingly small damping caused by the first phase of the corona.

If the probability of electrons becoming available before $k_5\tau$ is neglected, we may put

$$\mathrm{e}^{-k_5\tau/\sigma} = 1. \tag{4}$$

PHILOSOPHICAL TRANSACTIONS OF THE ROYAL SOCIETY A MATHEMATICAL, PHYSICAL & ENGINEERING SCIENCES

Then the probability of breakdown occurring under an impulse of wave front τ may be written as

$$P_1 = 1 + e^{-k_1\tau/\sigma} - e^{-k_2\tau/\sigma} + e^{-k_3\tau/\sigma} - e^{-k_4\tau/\sigma}; \quad (5)$$

and the probability of breakdown not resulting under the impulse is

$$P_2 = e^{-k_2\tau/\sigma} - e^{-k_1\tau/\sigma} + e^{-k_4\tau/\sigma} - e^{-k_3\tau/\sigma}. \quad (6)$$

These probability functions will result in the type of curve found in figure 8. The usefulness of the statistical approach is limited, however, since the corona form will depend not only upon the potential at which ionization begins, but also upon the subsequent rate of voltage rise. The k-factors are thus not fully independent of τ.

(iii) *Breakdown after long time lags*

The experiments carried out with the superimposition of potential upon an impulse already being applied to a rod/rod gap (§3(*b*) (ii)) clearly indicated that the electric gradient in the gap is varying with time. The form taken by the curves of percentage breakdown against time of step (figure 7) and the demonstrated existence of both short- and long-lag breakdown are fully compatible. The location of the minimum in figure 7 is an interesting confirmation of the limited conductivity of the negative corona channels as suggested by Brago & Stekolnikov (1958). It appears that not until about 15 μs after the growth of the corona is the net charge in the cathode region so distributed as to minimize the prevailing electric gradient.

The slow fall of breakdown strength after 15 μs is strongly indicative of drift of the space charge in the electric field. This period during the impulse application corresponds to the dead-time of the time-lag histograms. As was suggested in part I, the absence of ionization activity is more probably due to the prevention of the detachment process than the reduction of the field below that which would support cumulative ionization.

When high fields are restored in the gap, further ionization takes place. If this discharge should not result in breakdown, further moderation of the electric field occurs; this is suggested by the second minimum observed in figure 7. The final fall of breakdown probability beyond 350 μs is almost certainly due to the decay of the original applied impulse.

The time-resolved photographs of figure 9 show that the onset of anode and cathode discharges and long mid-gap streamers preceded long-lag breakdown in rod/rod gaps. Since no long time lags are observed in the rod/plane gap under negative impulses, it is probable that in rod/rod gaps the discharge from the rod anode initiates the process, although no time differences could be measured on the photographs.

5. Conclusions

(*a*) Negative impulse discharges can be subject to complete interruption of ionization activity similar in character to that shown to occur in the positive discharge, even when the potential difference across the gap is maintained. The resulting dead-time gives rise to total time lags much longer than the sum of the statistical time lag and the formative time-lag.

(*b*) The variation of time-lag characteristics with the impulse wave form and with gap size and geometry shows many marked differences from those observed with positive impulses. The principal contrasts are that long time lags occur under negative impulses for

all rod/rod gaps but never for rod/plane gaps; for positive impulses they were observed over the same range of gap lengths for both rod/rod and rod/plane gaps.

(*c*) The dead-time of the time-lag observations is ascribed to the effect of the corona space charge; an experimental examination of the variation of breakdown strength of the gap during the impulse supports this view. Many of the time-lag features of (*b*) can be understood from a study of the corona behaviour.

(*d*) The form of the negative impulse corona discharge from a rod electrode is critically dependent upon the rate of rise of the applied potential. The most prominent variations can be understood in terms of self-quenching due to space charge modification of the applied field.

(*e*) The positive leader is observed to form before the negative leader under many conditions. This is always the case when the anode leader is formed due to the increased electric field induced at the anode by the negative corona phase. When the induced field is insufficient to initiate breakdown, as for example with a plane anode, the positive leader is initiated from the point of contact of the negative corona channels with the anode. The positive and negative leader onset then appears simultaneous.

(*f*) If initiation of the anode leader is accepted as the criterion of breakdown, many observed variations of breakdown voltage with wave shape and gap system can be accounted for in terms of corona characteristics.

(*g*) The geometry of the earthed electrode is of greater influence in determining the breakdown strength of the gap in the negative discharge than in the positive discharge. This is also true of the influence of the impulse wave front.

Appendix I. The superimposed-impulse circuit

For simplification both the impulse generator wave-tail resistor (0·7 MΩ, not shown in figure 1), and R_4 (1·6 MΩ) are considered infinite. The equation for V_2 subsequent to the breakdown of G_1, G_2 and G_3 is

$$K_1\frac{\mathrm{d}^3V_2}{\mathrm{d}t^3}+K_2\frac{\mathrm{d}^2V_2}{\mathrm{d}t^2}+K_3\frac{\mathrm{d}V_2}{\mathrm{d}t}=0, \tag{7}$$

where

$$K_1=C_1C_3C_4C_6R_5, \tag{8}$$

$$K_2=C_1C_6(C_3+C_4)+\frac{C_4R_5}{R_6}\{C_g(C_3+C_6)+C_3C_6\}, \tag{9}$$

and

$$K_3=\frac{1}{R_6}\{C_g(C_3+C_4+C_6)+C_6(C_3+C_4)\}. \tag{10}$$

Equation (7) has a solution of the form

$$V_2=L\,\mathrm{e}^{-\alpha t}+M\,\mathrm{e}^{-\beta t}+N, \tag{11}$$

where

$$\alpha,\ \beta=-\frac{K_2}{2K_1}\pm\left(\frac{K_2^2}{4K_1^2}-\frac{K_3}{K_1}\right)^{\frac{1}{2}}, \tag{12}$$

$$L=\frac{1}{\alpha-\beta}\left[\frac{\overline{V}_4-\overline{V}_3}{C_3R_5}-\frac{C_3+C_6}{C_3C_6R_6}(\overline{V}_2-\overline{V}_1)+\beta(N-\overline{V}_2)\right], \tag{13}$$

$$M=\overline{V}_2-N-L, \tag{14}$$

and

$$N=\frac{(C_g\overline{V}_1+[C_3C_6/(C_3+C_6)]\overline{V}_2)\,(C_3+C_4+C_6)+C_4C_6\overline{V}_4}{(C_g+C_6)\,(C_3+C_4+C_6)-C_6^2}. \tag{15}$$

$\bar{V}_1$, $\bar{V}_2$, $\bar{V}_3$ and $\bar{V}_4$ are values at a time T on the wave tail of the primary impulse immediately preceding the collapse of G_1, G_2 and G_3.

It can be shown that

$$\bar{V}_1 = nV_0\,[\mathrm{e}^{-\alpha' t} - P(\mathrm{e}^{-\alpha' t} - \mathrm{e}^{-\beta' t})], \tag{16}$$

$$\bar{V}_2 = \frac{nV_0}{C_2 R_6(\beta' - \alpha')}\,(\mathrm{e}^{-\alpha' t} - \mathrm{e}^{-\beta' t}), \tag{17}$$

$$\bar{V}_3 = \bar{V}_2\left(\frac{C_6}{C_3 + C_6}\right), \tag{18}$$

and

$$\bar{V}_4 = V_0. \tag{19}$$

α', β' and P are constants depending on the circuit values. In this case the impulse generator wave tail resistor is included in the analysis. n is the number of stages in the impulse generator and V_0 the steady charging voltage.

The rise time of the superimposed impulse is given by

$$t_1 = \frac{1}{\alpha - \beta}\ln\left[-\frac{\beta M}{\alpha L}\right] \tag{20}$$

and the maximum value of V_2 by

$$V_c = L\,\mathrm{e}^{-\alpha t_1} + M\,\mathrm{e}^{-\beta t_1} + N. \tag{21}$$

For a three-stage impulse generator of discharge capacitance $3{\cdot}5 \times 10^{-9}$ F, $C_6 = 3{\cdot}5 \times 10^{-10}$ F and $R_6 = 1{\cdot}87$ kΩ, the superimposed impulse amplitude was calculated for various values of C_3 and C_4 (table 1). For a given value of C_4 there is an optimum value of C_3 to give maximum amplitude.

TABLE 1

C_3 (F)	C_4 (F)	t_1 (μs)	step pulse height $V_c - \bar{V}_2$	percentage rise of V_2 due to step pulse
10^{-8}	4×10^{-8}	0·76	0·24 V_0	8·9
$5{\cdot}0 \times 10^{-9}$	3×10^{-8}	0·55	0·32 V_0	11·7
$3{\cdot}3 \times 10^{-9}$	2×10^{-8}	0·47	0·35 V_0	12·8
$2{\cdot}5 \times 10^{-9}$	10^{-8}	0·34	0·30 V_0	11·0

APPENDIX II. TIME-RESOLVED PHOTOGRAPHY OF THE BREAKDOWN OF A 76·2 CM ROD/ROD GAP AT 530 KV

Figure 9 (*a*) shows the type of discharge obtained with an impulse wave front of 0·20 μs. The corona discharge at each electrode was coincident at a time near zero and extended 14 cm from the cathode and 11 cm from the anode. In this instance further discharges, extending about half-way across the gap, occurred from the cathode at times of 2·25 and 3·95 μs. The anode leader from the earthed rod was initiated at 4·75 μs and the cathode leader at 6·2 μs. It was typical of the glow discharge which spanned the gap and was associated with the leader channels that its diameter was less in the region ahead of the negative leader than that in the anode half of the gap.

Figure 9 (*b*) illustrates a failure of the gap to break down when the impulse wave front was 0·35 μs. The radius of the negative corona, although similar in structure to that at the 0·20 μs wave front, was reduced to 8 cm; the anode corona extent was 7·5 cm.

The third wave front used was of duration 0·50 μs. Figure 9 (*c*) shows a breakdown of time lag 7·35 μs. The corona phase exhibited the dual structure of forward-developing and retrograde streamers which was noted earlier. The negative corona extended to 22 cm and the positive to 10 cm. A small discharge from the cathode at 2·45 μs was followed by the development of the anode leader at 3·35 μs and the cathode leader at 3·85 μs. Many more breakdowns of long time lag were found with 0·50 μs wave front than with 0·20 μs wave front. The breakdown of figure 9 (*d*) occurred following a delay of 190 μs. In order to record the moment of arrest on the film at the high rotating-mirror speed employed, the synchronization of the mirror and the triggering of the impulse generator had to be offset by some 200 μs. Thus the corona phase near time zero of this breakdown is not present in the figure. A small shaft of discharge occurred at the cathode at 183·5 μs, and the anode and cathode leaders developed at 184·5 and 185 μs respectively.

Impulses of wave front 0·65 μs produced breakdowns of the kind reproduced in figure 9 (*e*). The negative corona consisted of forward streamers 4 cm in extent and retrograde streamers 19·5 cm long. The retrograde streamers terminated nearer the cathode than at slightly slower wave fronts. The anode corona occurred with no discernible delay and extended 10·5 cm into the gap. Further discharges from the cathode appeared to be associated with mid-gap channels with cathode-directed branching. The negative leader commenced at 6·9 μs, the positive at 6·5 μs, and the discharge was arrested at 12·0 μs.

Figure 9 (*f*) is a typical corona discharge produced at 0·90 μs wave front. This impulse failed to cause breakdown of the gap. The overall extent of the negative and positive corona was rather less than was produced by the 0·65 μs wave front; the negative corona was 15 cm long, and the positive 9·5 cm. The hemisphere of initial streamers was merely 2·5 cm in radius.

This latter phase is not seen in figure 9(*g*), which is a photograph obtained with a 1·35 μs wave front. The retrograde streamers were more numerous than for slower wave fronts and extended for 16·5 cm. The anode corona terminated 14 cm from the electrode. This was followed by a breakdown in 110 μs which is not shown. Figure 9 (*h*) shows the final stages of a discharge of time lag 190 μs. A straight, intense discharge developed from the cathode at 177·5 μs and extended 1·5 cm into the gap. Associated with this was a long, fairly straight mid-gap channel of overall length 22 cm, branched towards the cathode at its upper end, and a small discharge from the anode surface. Further discharges occurred from the cathode along the same path as the original channel, and in each case the mid-gap channel was regenerated and extended further in the direction of this earthed anode. The anode and cathode leader channels appeared to initiate simultaneously at 183 μs, but the initial velocity of the positive leader was $3{\cdot}6 \times 10^6$ cm/s compared with the negative leader velocity of $4{\cdot}4 \times 10^5$ cm/s. The starting point of the negative leader was from the tip of the original cathode channel.

With a wave front of 1·95 μs many of the retrograde negative corona channels originated between 4 and 13 cm from the cathode (figure 9 (*i*)). These were frequently connected to the cathode by bundles of fine channels. Breakdown followed in this case after 145 μs. Again most breakdowns were of long time lag, the time lag of the discharge of figure 9 (*j*) being 130 μs. The form was similar to that of figure 9 (*h*), but in this case the positive leader precedes the negative by 1 μs.

PHILOSOPHICAL TRANSACTIONS OF THE ROYAL SOCIETY A MATHEMATICAL, PHYSICAL & ENGINEERING SCIENCES

References

Allibone, T. E. 1937 *J. Instn Elect. Engrs*, **81**, 741.
Allibone, T. E., Hawley, W. G. & Perry, F. R. 1934 *J. Instn Elect. Engrs*, **75**, 670.
Allibone, T. E. & Meek, J. M. 1938 *Proc. Roy. Soc.* A, **166**, 97.
American Institute of Electrical Engineers standards no. 4. 1940.
Bellaschi, P. L. & Teague, W. L. 1934 *Elect. Engng*, **53**, 1638.
Brago, E. N. & Stekolnikov, I. S. 1958 *Izv. Akad. Nauk SSSR, O.T.N.* **11**, 50.
Gorev, A. A., Zalesky, A. M. & Riabov, B. M. 1948 *Conf. Int. Gr. Res. Elect.* paper no. 142.
Loeb, L. B. 1935 *Phys. Rev.* **48**, 684.
Park, J. H. & Cones, N. H. 1956 *Bur. Stand. J. Res., Wash.*, **56**, 201.
Stekolnikov, I. S. & Shkilev, A. V. 1962 *Dokl. Akad. Nauk SSSR*, **145**, 782.
Waters, R. T. & Jones, R. E. 1959 *Proc. Fourth Int. Conf. on Ionization Phenomena in Gases*. North-Holland Publishing Company.

PHILOSOPHICAL TRANSACTIONS OF THE ROYAL SOCIETY A MATHEMATICAL, PHYSICAL & ENGINEERING SCIENCES

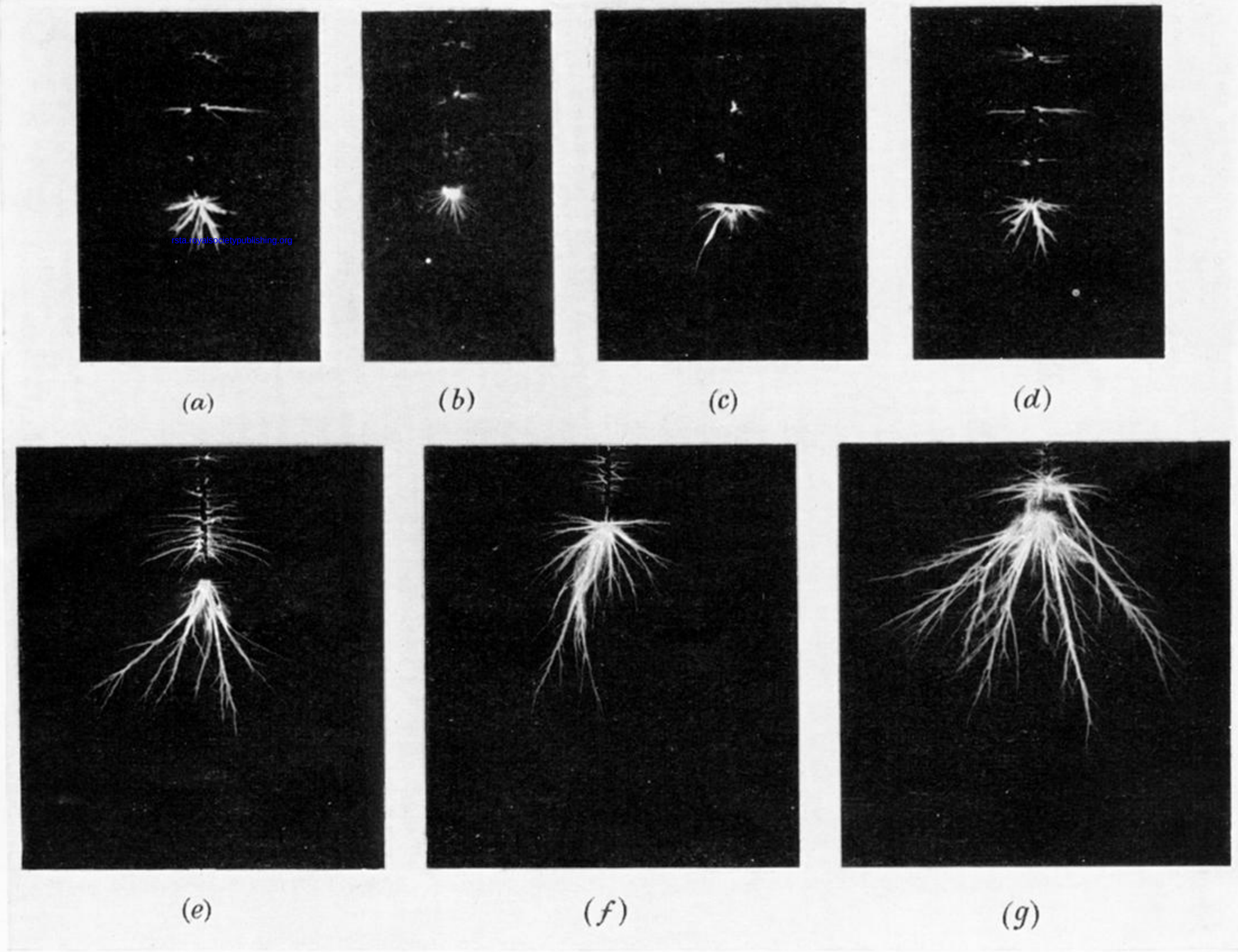

FIGURE 2. Impulse corona discharge at a rod-cathode: (*a*) 250 kV crest voltage, wave shape 0·20/2000 μs; (*b*) 250 kV crest voltage, wave shape 0·50/2000 μs; (*c*) 310 kV crest voltage, wave shape 0·50/2000 μs; (*d*) 310 kV crest voltage, wave shape 0·20/2000 μs; (*e*) 540 kV crest voltage, wave shape 0·50/2000 μs; (*f*) 700 kV crest voltage, wave shape 0·20/2000 μs; (*g*) 700 kV crest voltage, wave shape 0·50/2000 μs.

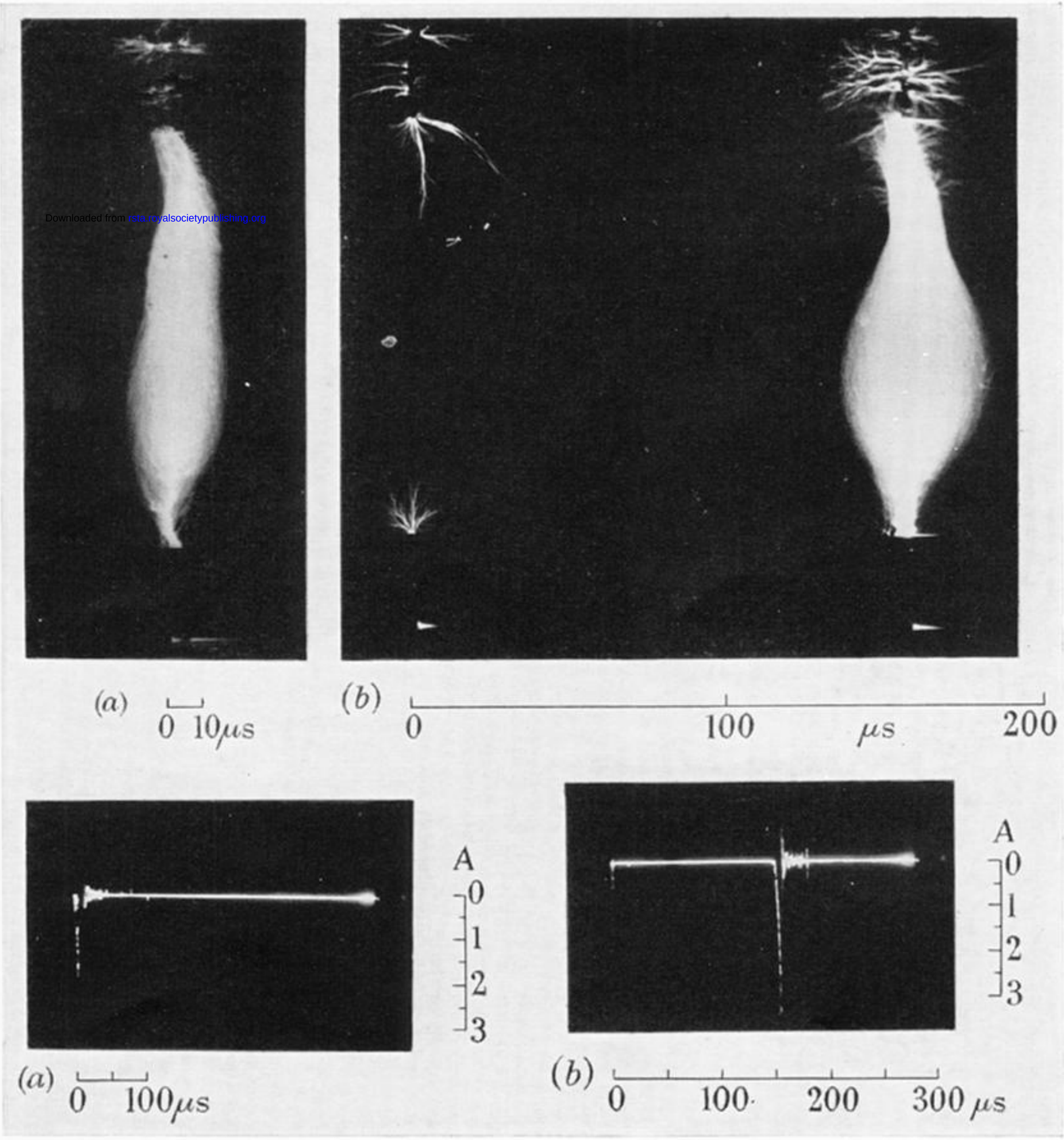

FIGURE 5. Time-resolved photographs of arrested breakdown in a 60 cm rod/rod gap for 440 kV crest voltage, wave shape 0·50/2000 μs.

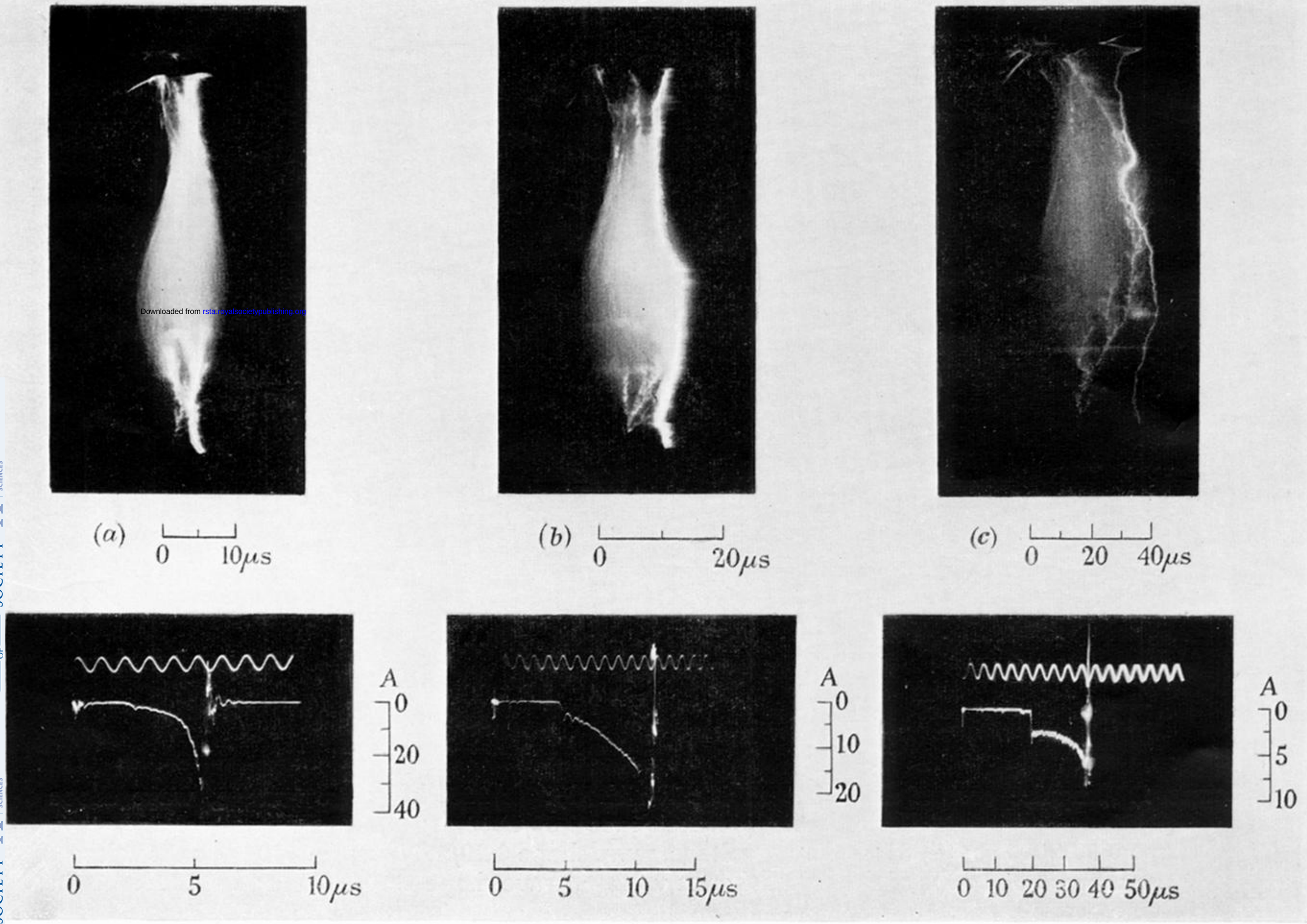

FIGURE 6. Time-resolved photographs of breakdown in a 106·7 cm rod/rod gap with increasing series resistance: (*a*) 790 kV crest voltage, added series resistance = 0 Ω; (*b*) 890 kV crest voltage, added series resistance = 20·5 kΩ; (*c*) 940 kV crest voltage, added series resistance = 200 kΩ.

PHILOSOPHICAL TRANSACTIONS OF THE ROYAL SOCIETY A MATHEMATICAL, PHYSICAL & ENGINEERING SCIENCES

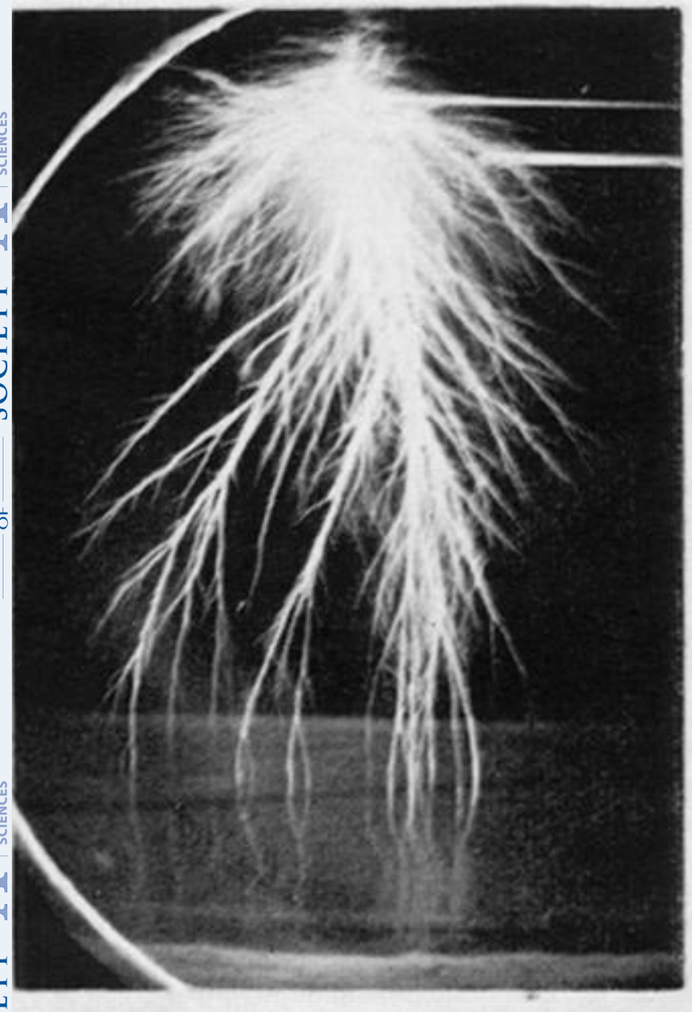

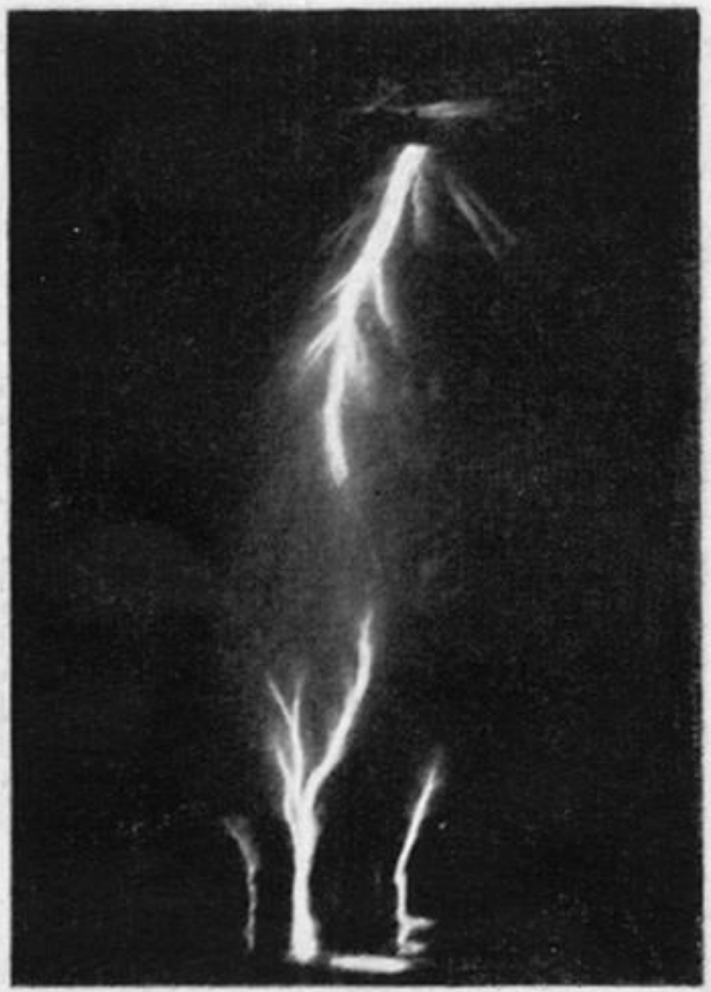

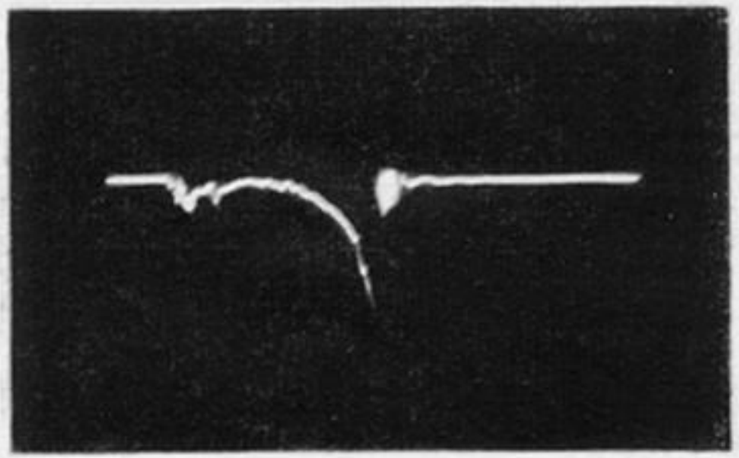

FIGURE 12. Time-resolved photographs of arrested breakdown in a 92 cm rod/plane gap for 1 MV crest voltage; wave shape 0·50/2000 μs.

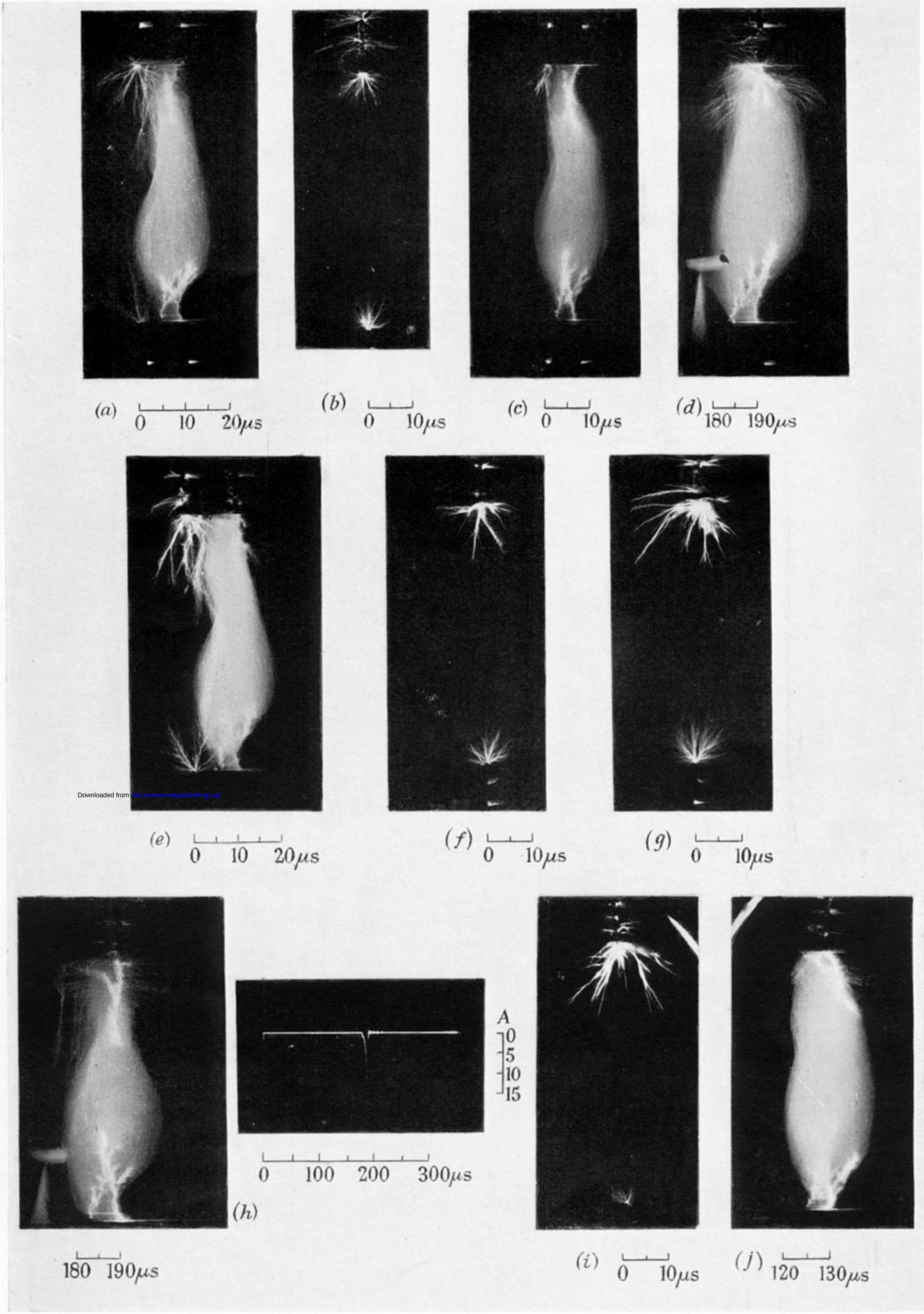

FIGURE 9. Time-resolved photographs of arrested breakdown in a 76·2 cm rod/rod gap with impulses of various wave front for 530 kV crest voltage. Wave shape: (*a*) 0·20/2000 μs; (*b*) 0·35/2000 μs; (*c*) 0·50/2000 μs; (*d*) 0·50/2000 μs; (*e*) 0·65/2000 μs; (*f*) 0·90/2000 μs; (*g*) 1·35/2000 μs; (*h*) 1·35/2000 μs; (*i*) 1·95/2000 μs; (*j*) 1·95/2000 μs.

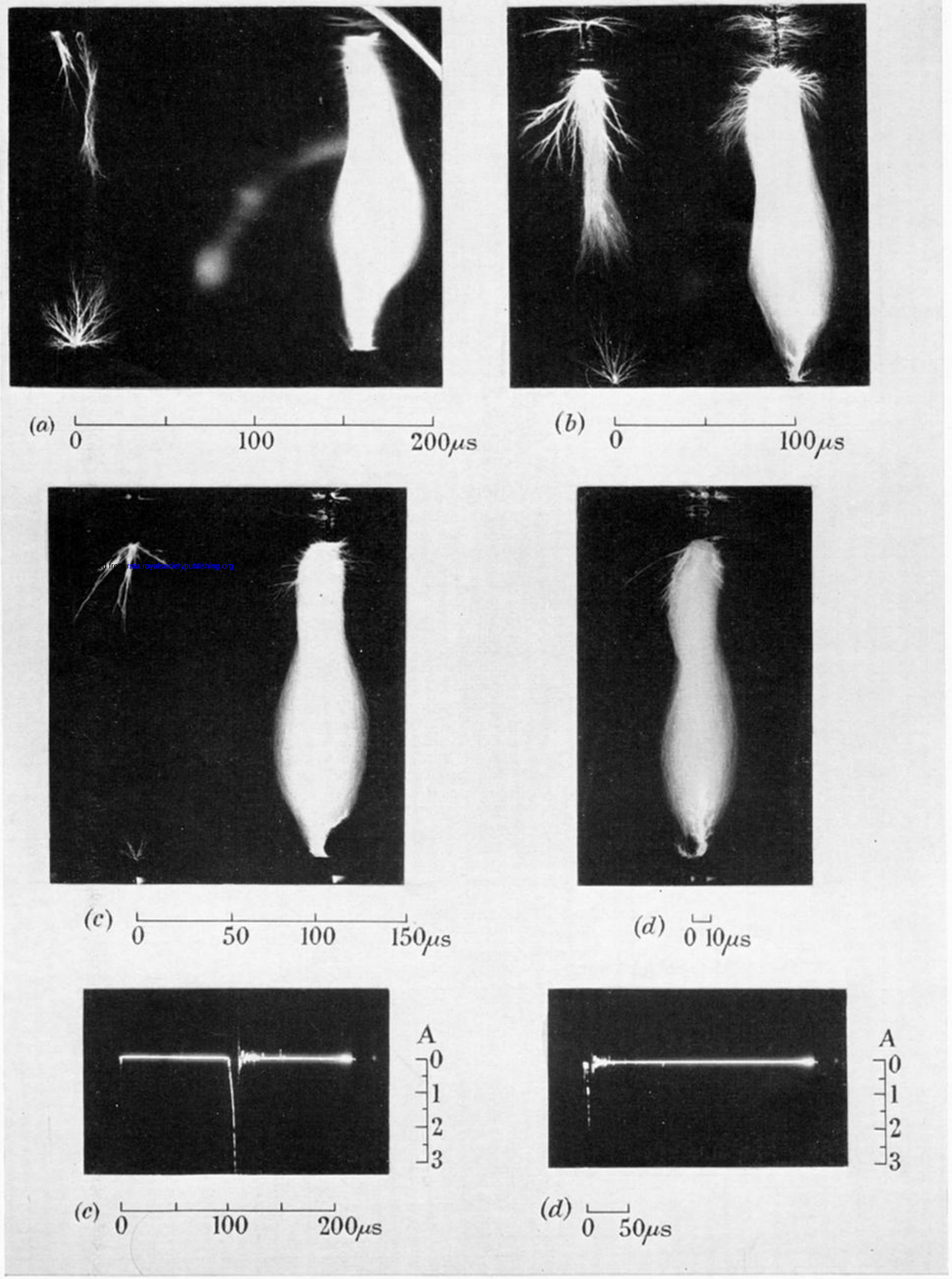

FIGURE 14. Time-resolved photographs of arrested breakdown in an 80 cm rod/rod gap for 550 kV crest voltage; wave shape 0·50/2000 μs.

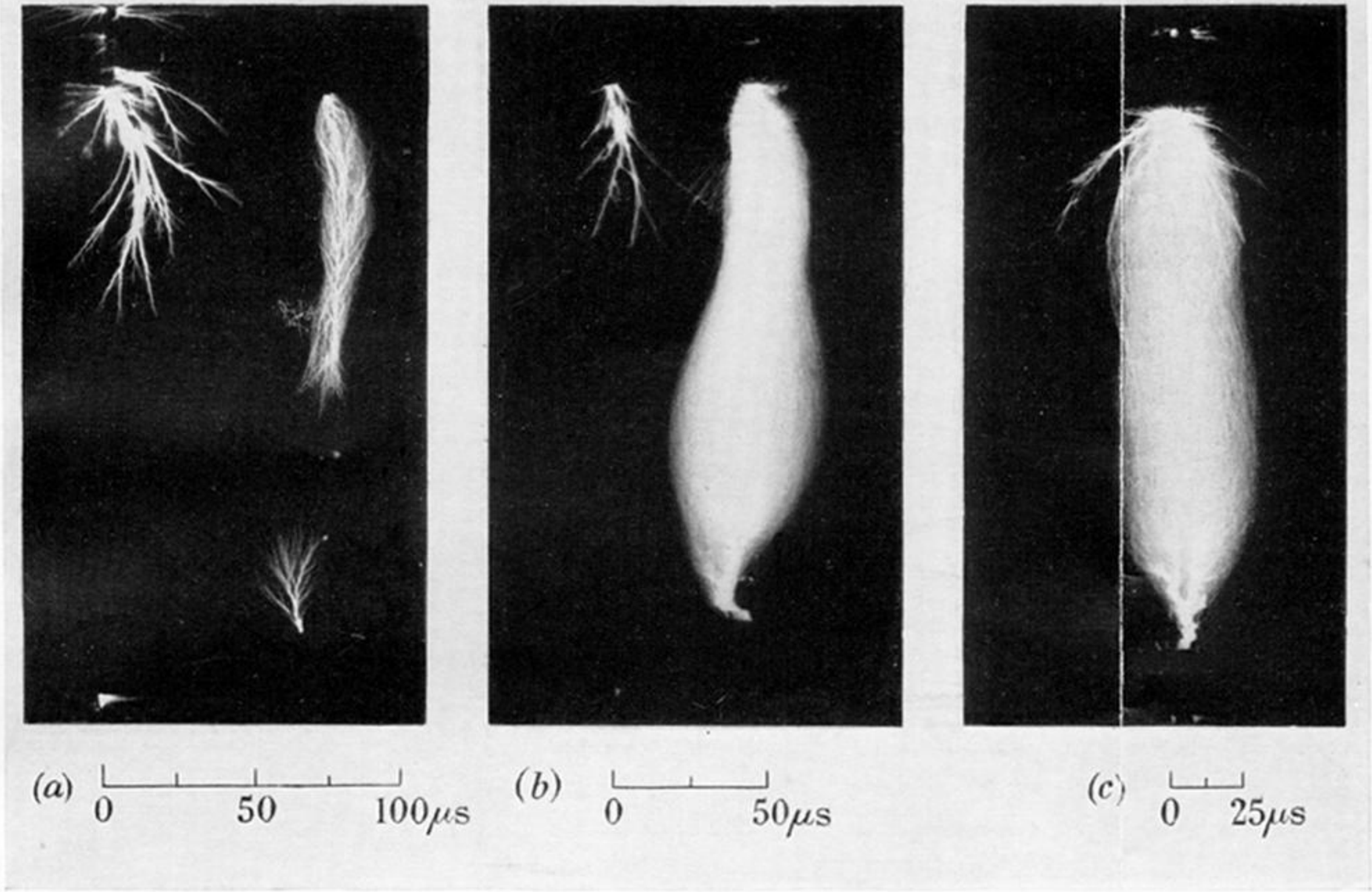

FIGURE 15. Time-resolved photographs of arrested breakdown in an 80 cm rod/6·25 cm diameter sphere gap for 570 kV crest voltage; wave shape 0·50/2000 μs.

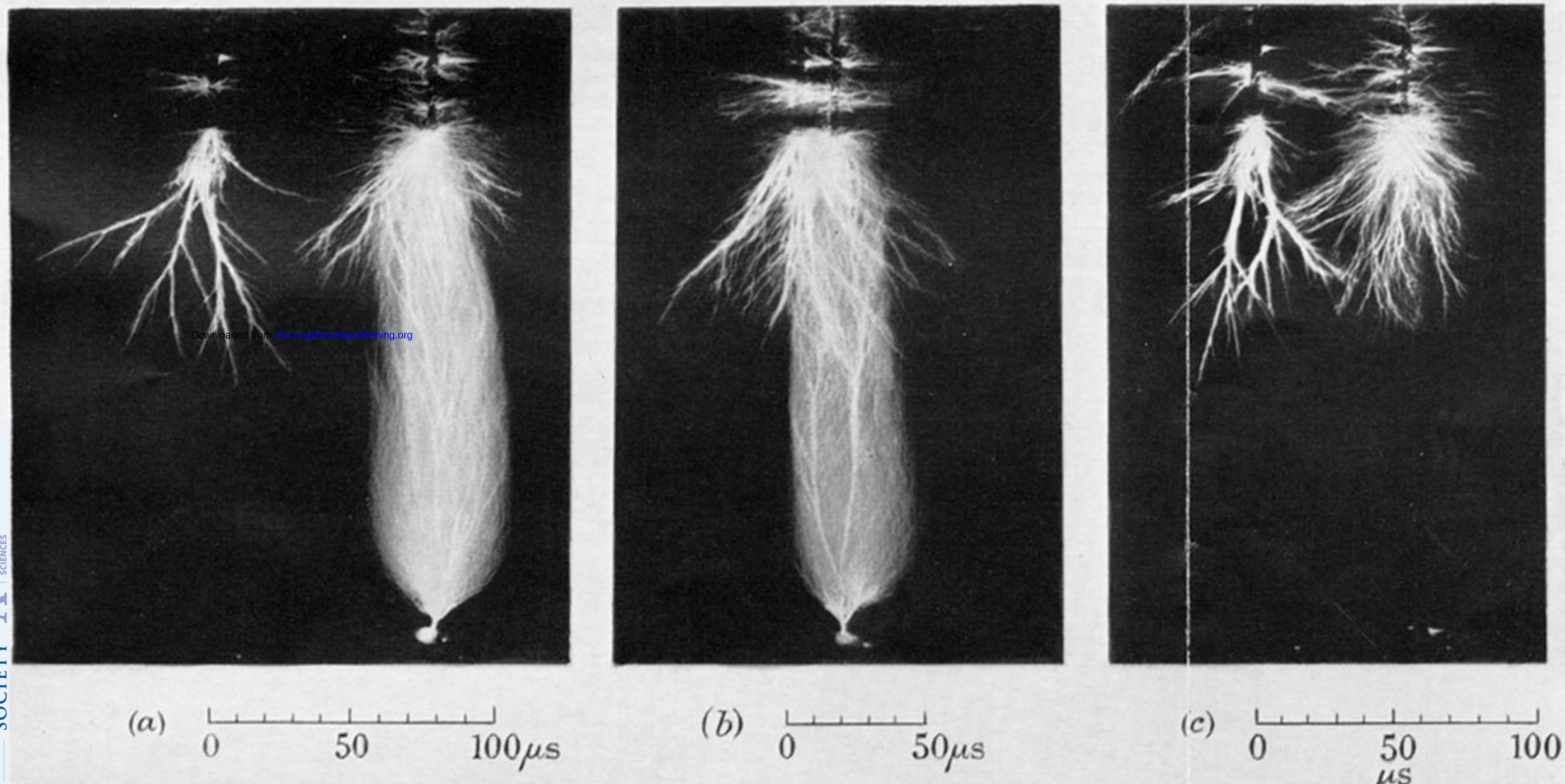

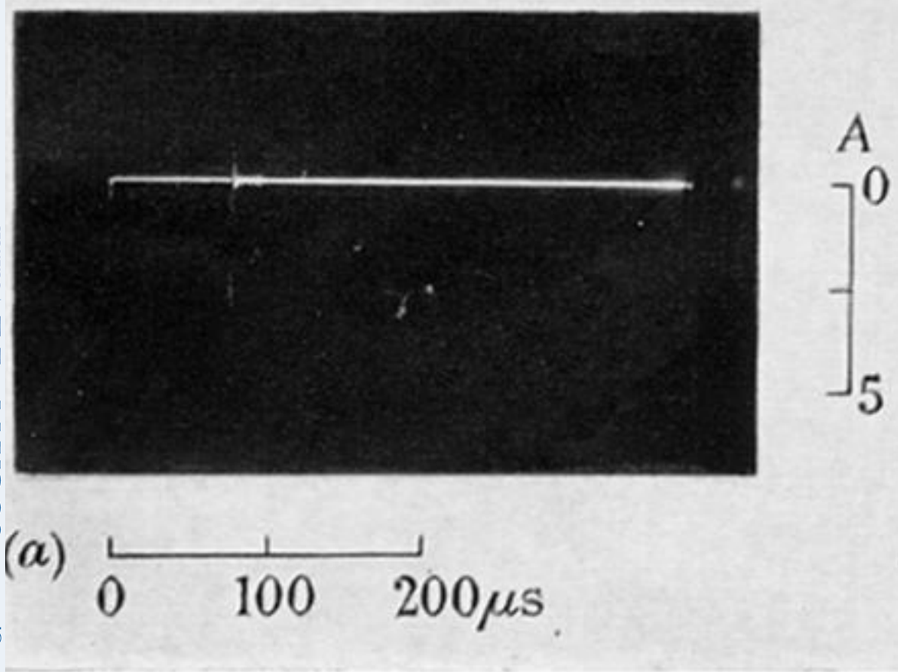

FIGURE 16. Time-resolved photographs of arrested breakdown in an 80 cm rod/12·5 cm diameter sphere gap for 710 kV crest voltage; wave shape 0·50/2000 μs.

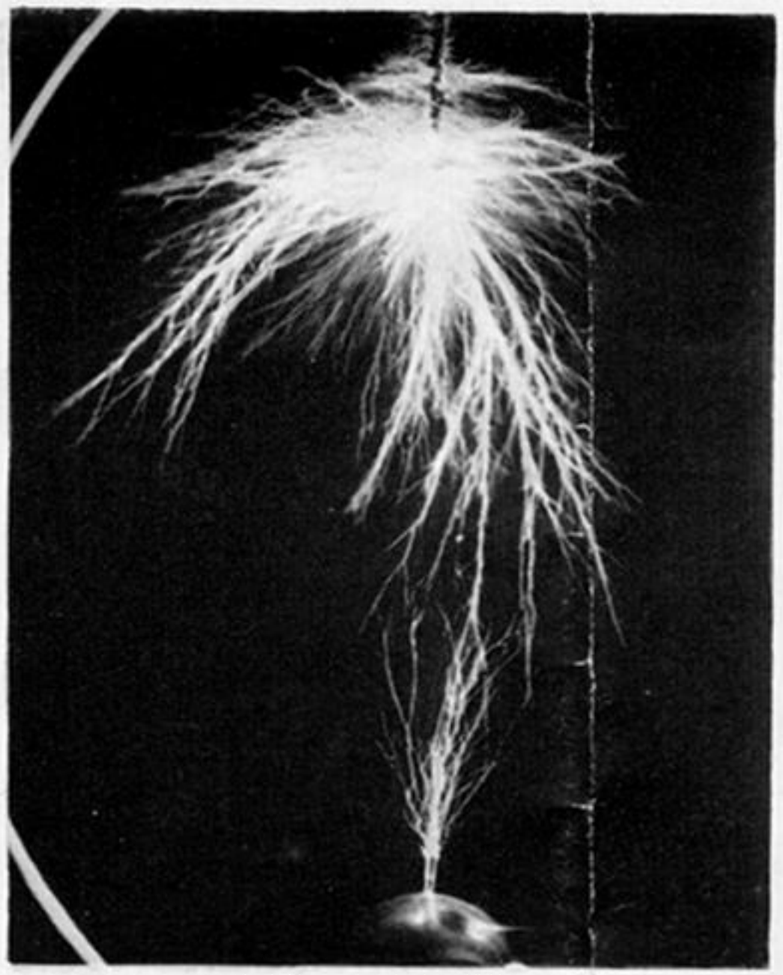

(a) 0 50μs

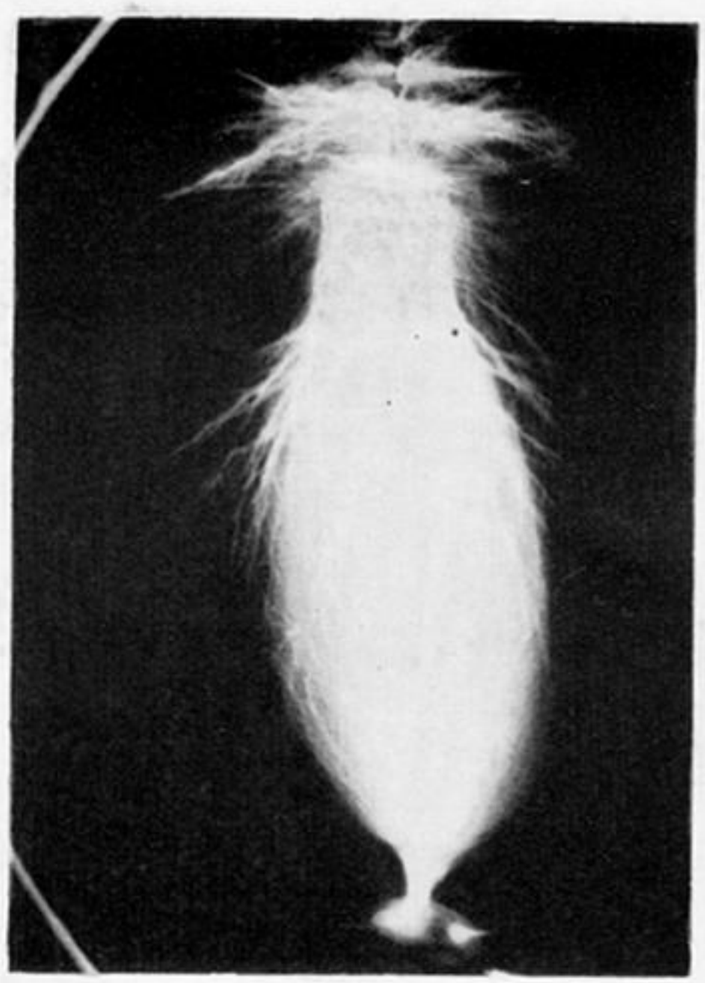

(b) 0 50μs

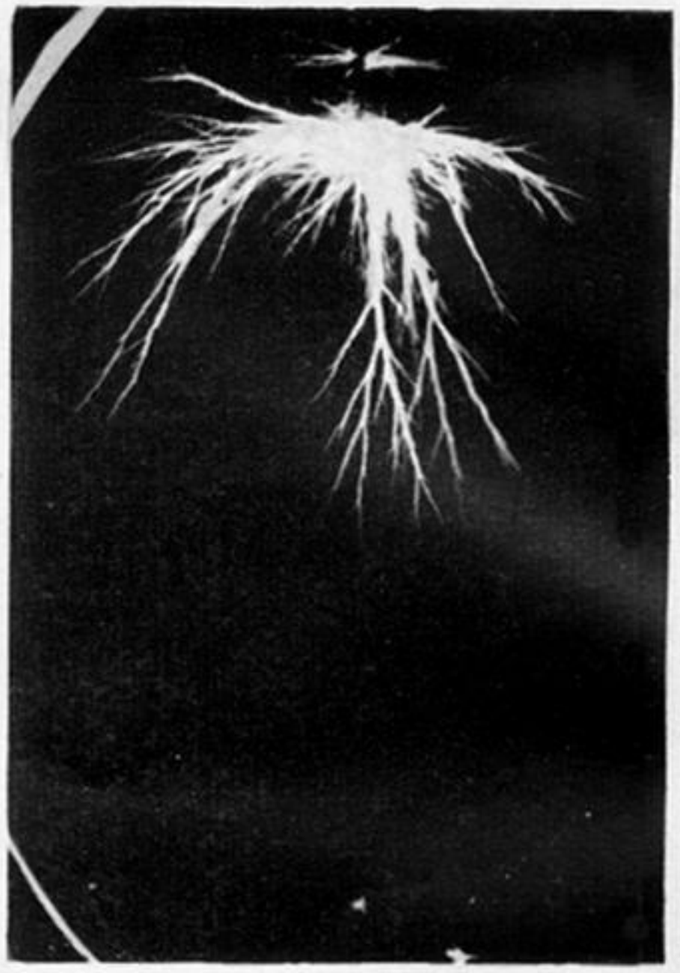

(d) 0 50μs

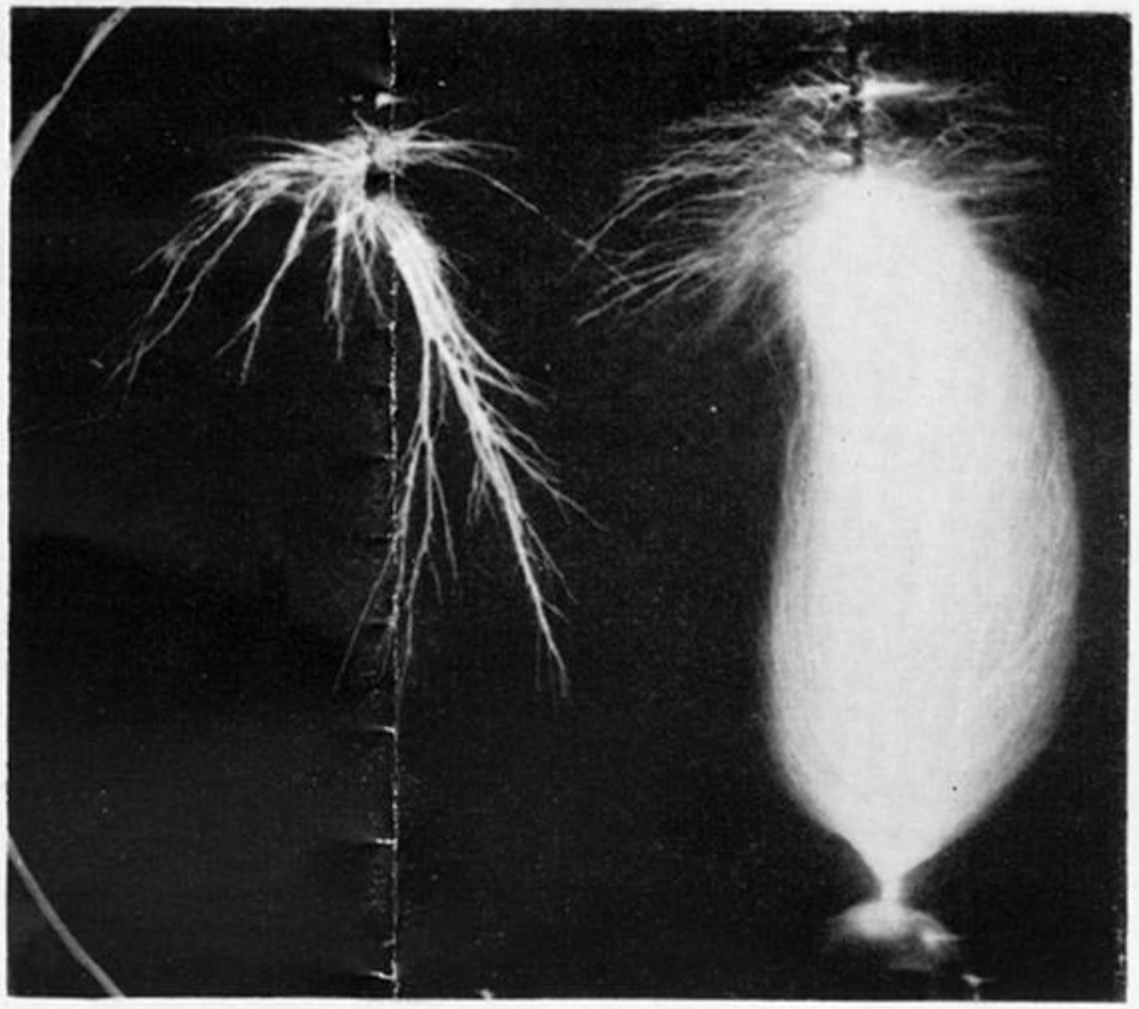

(c) 0 50 100 150μs

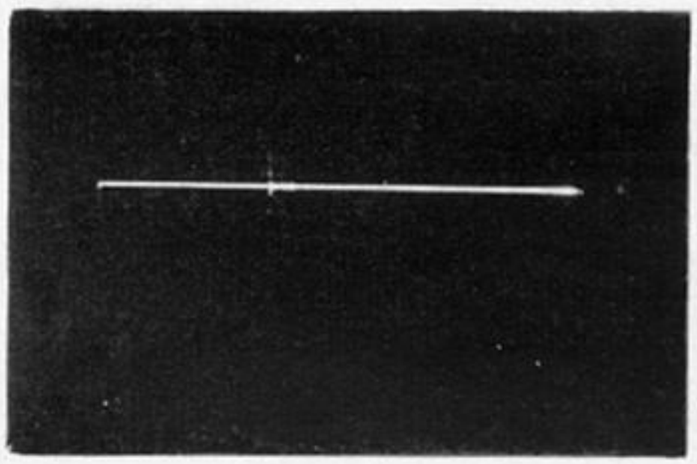

A 0 5

(c) 0 100 200μs

FIGURE 17. Time-resolved photographs of arrested breakdown in an 80 cm rod/25 cm diameter sphere gap for 860 kV crest voltage; wave shape 0·50/2000 μs.

PHILOSOPHICAL TRANSACTIONS OF THE ROYAL SOCIETY A MATHEMATICAL, PHYSICAL & ENGINEERING SCIENCES

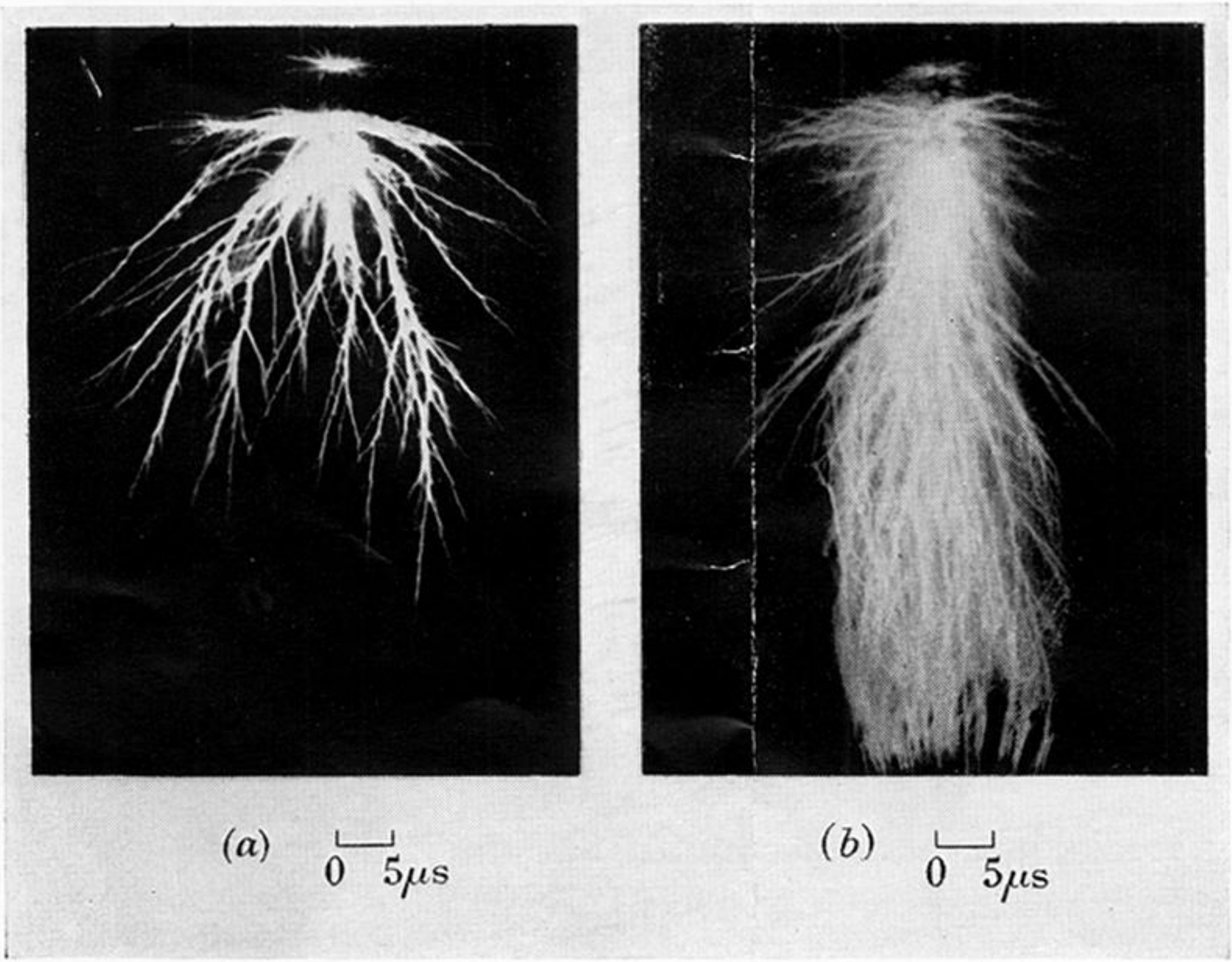

IGURE 18. Time-resolved photographs of arrested breakdown in an 80 cm rod/75 cm diameter sphere gap; wave shape 0·50/2000 μs; (*a*) 830 kV crest voltage, (*b*) 900 kV crest voltage.

PHILOSOPHICAL TRANSACTIONS OF THE ROYAL SOCIETY A MATHEMATICAL, PHYSICAL & ENGINEERING SCIENCES

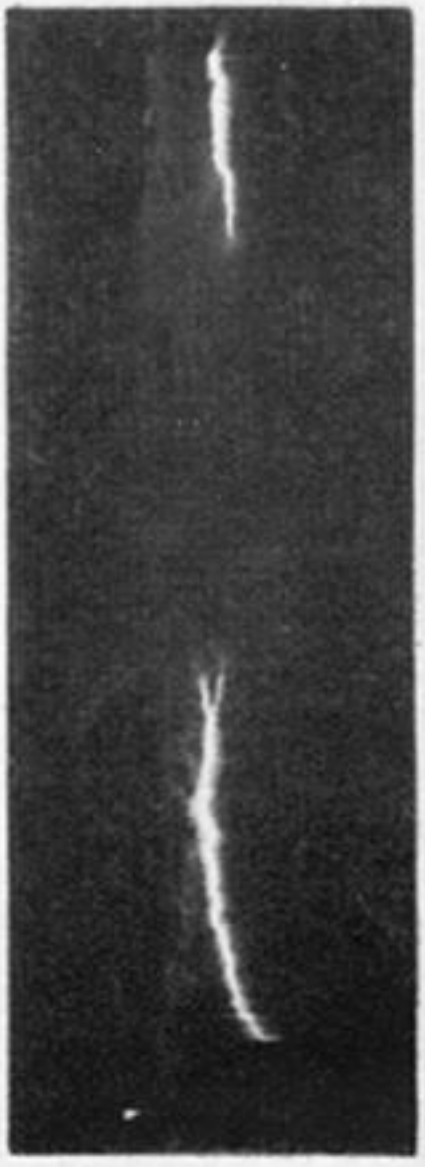

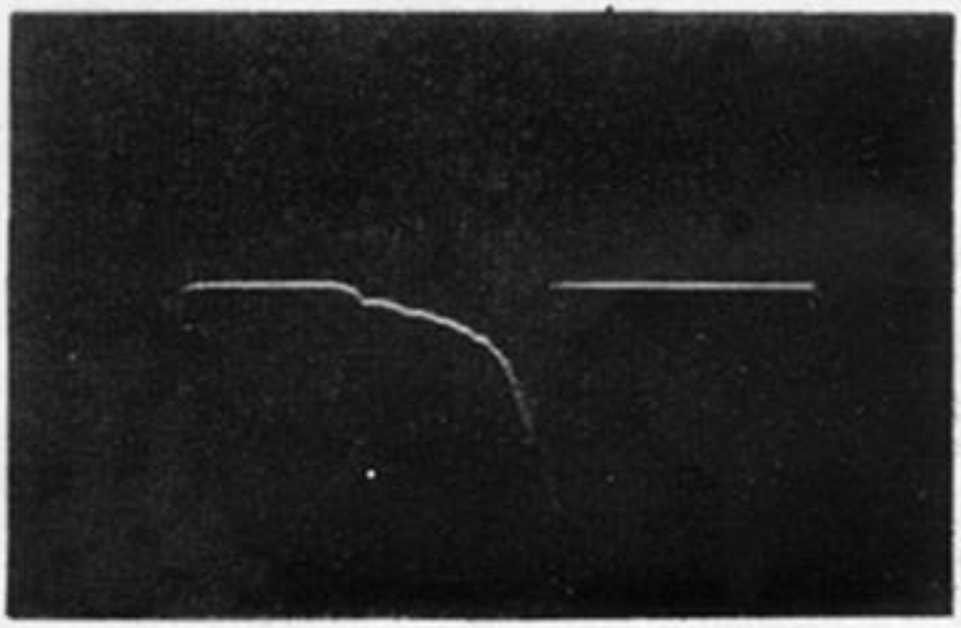

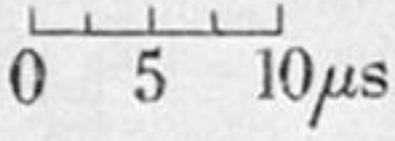

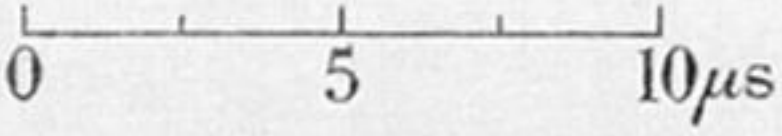

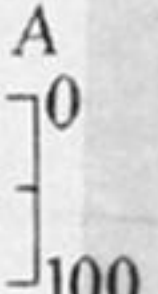

IGURE 19. Time-resolved photograph of arrested breakdown in a 75 cm diameter sphere/rod gap for 860 kV crest voltage; gap spacing 106·7 cm; wave shape 0·50/2000 μs.